Front. Phys. 11(3), 118102 (2016)
DOI 10.1007/s11467-015-0529-2

REVIEW ARTICLE

Two-body physics in quasi-low-dimensional atomic gases under spin–orbit coupling

Jing-Kun Wang[1,2], **Wei Yi**[3,4,*], **Wei Zhang**[1,2,†]

[1] *Department of Physics, Renmin University of China, Beijing 100872, China*
[2] *Beijing Key Laboratory of Opto-electronic Functional Materials and Micro-nano Devices, Renmin University of China, Beijing 100872, China*
[3] *Key Laboratory of Quantum Information, University of Science and Technology of China, Chinese Academy of Sciences, Hefei 230026, China*
[4] *Synergetic Innovation Center of Quantum Information and Quantum Physics, University of Science and Technology of China, Hefei 230026, China*
*Corresponding authors. E-mail: * wyiz@ustc.edu.cn, † wzhangl@ruc.edu.cn*
Received August 15, 2015; accepted October 25, 2015

One of the most dynamic directions in ultracold atomic gas research is the study of low-dimensional physics in quasi-low-dimensional geometries, where atoms are confined in strongly anisotropic traps. Recently, interest has significantly intensified with the realization of synthetic spin–orbit coupling (SOC). As a first step toward understanding the SOC effect in quasi-low-dimensional systems, the solution of two-body problems in different trapping geometries and different types of SOC has attracted great attention in the past few years. In this review, we discuss both the scattering-state and the bound-state solutions of two-body problems in quasi-one and quasi-two dimensions. We show that the degrees of freedom in tightly confined dimensions, in particular with the presence of SOC, may significantly affect system properties. Specifically, in a quasi-one-dimensional atomic gas, a one-dimensional SOC can shift the positions of confinement-induced resonances whereas, in quasi-two-dimensional gases, a Rashba-type SOC tends to increase the two-body binding energy, such that more excited states in the tightly confined direction are occupied and the system is driven further away from a purely two-dimensional gas. The effects of the excited states can be incorporated by adopting an effective low-dimensional Hamiltonian having the form of a two-channel model. With the bare parameters fixed by two-body solutions, this effective Hamiltonian leads to qualitatively different many-body properties compared to a purely low-dimensional model.

Keywords artificial gauge field, synthetic spin–orbit coupling, quasi-low dimensional sysem

PACS numbers 81.05.Uw, 68.37.-d, 73.20.-r

Contents

*Specail Topic: Artificial Gauge Field in Ultra-Cold Atomic Gases (Eds. Shuai Chen, Carlos SadeMelo, Chuanwei Zhang & Peng Zhang).

1 Introduction

Synthetic spin–orbit coupling (SOC) in ultracold atomic gases has stimulated much interest following its experimental realization [1–9]. Recent theoretical studies have revealed the existence of various exotic many-body states in ultracold atoms with SOC [10–17]. These interesting many-body states typically do not have direct counterparts in condensed-matter systems, although they often share similarities with relevant phases in condensed-matter systems such as topological superconductors or Weyl semimetals [15–17]. A key advantage of studying novel many-body states with cold atomic gases is their highly tunable parameters, such as the interaction strength, form and strength of the synthetic SOC, and system geometry. While the flexible control greatly extends the horizon of quantum simulation in cold atomic gases, fresh questions and challenges arise over properties of the system within new parameter regimes.

A particularly important case is the understanding of few-body physics in spin–orbit coupled atomic gases. Because few-body processes constitute the basic building blocks of an interacting many-body system, important physical insights can be gleaned by careful examinations of few-body problems. While previous studies entailed investigation of the effects of SOC on two-body scattering processes with short-range potentials in various spatial dimensions [18–21], interesting SOC-induced two- and three-body bound states have also been reported recently [22–24]. Furthermore, because SOC is expected to induce topologically nontrivial phases in spatial dimensions lower than three [25], the study of few-body problems in quasi-low spatial dimensions may shed light on the possibility of generating topological matter. In cold atomic gases, quasi-low-dimensional geometry is typically achieved by strongly anisotropic confinements. In tightly confined spatial dimensions, atomic motion is expected to be discretized. In principle, these discrete degrees of freedom can be integrated out, which leaves the resulting system effectively low dimensional. However, recent studies have revealed that it is difficult to do so when the two-body binding energy becomes large [26, 27]. In this case, a spectrum of low-lying discrete states in the tightly confined directions can be populated, which makes a direct integration intractable. Although this can be the case for strongly interacting atomic gases in general, the situation can be even worse in the presence of synthetic SOC, which typically enhances the two-body binding energy [28, 29]. The observations above necessitate a better understanding of the quasi-low-dimensional condition in cold atomic gases under synthetic SOC, as well as a more careful treatment of these systems. This can be done by a systematic investigation of the properties of two-body bound states in a cold atomic gas with quasi-low-dimensional geometry.

In this paper, we review recent progresses on the study of two-body physics in a quasi-low-dimensional cold atomic gas under synthetic SOC. Our goal is twofold. First, by presenting and comparing two-body physics both with and without SOC, we reveal the key impacts of SOC on quasi-low-dimensional atomic gases. In particular, we discuss the effects of SOC on physical processes of two-body binding and scattering and on the confinement-induced resonance (CIR) in these systems. We argue that the population of the discrete states in the tightly confined directions raises the important question as to the appropriate low-dimensional model one must adopt to characterize quasi-low-dimensional systems. Second, we review a practical solution in which the system can be modeled using an effective low-energy Hamiltonian in low spatial dimensions. The effective Hamiltonian takes the form of a two-channel model, where population in the tightly confined directions are bundled with the two-body bound states and modeled by a structureless dressed molecular mode. We first review the derivation and application of the effective two-channel Hamiltonian in the absence of SOC and then focus on its application in quasi-low dimensions in the presence of SOC.

The paper is organized as the follows: In Section 2, we review two-body physics in quasi-one and quasi-two dimensions without SOC, focusing on CIR and the population of the excited states in the tightly confined directions. In Section 3, we present two-body physics in quasi-one and quasi-two dimensions in the presence of SOC. We then discuss a practical way to introduce an effective two-channel model for the characterization of these quasi-low-dimensional systems. In Section 4, we review the derivation of the effective two-channel model both without and with SOC. In this section, we also discuss the application of the effective two-channel model, where we find that, fortunately, the inclusion of excited modes in the tightly confined direction actually helps to stabilize the topological superfluid state in a quasi-two-dimensional Fermi gas under Rashba SOC and an effective Zeeman field. Finally, we summarize our work in Section 5.

2 Two-body physics in quasi-low dimensions without SOC

In this section, we will review two-body problems in quasi-one and quasi-two dimensions in the absence of SOC. Discussions on both the bound states and the scattering states will be included in this section [30–42]. Specifically, we will introduce the exact solutions of the two-body bound states and calculate the zero-energy scattering amplitude of the scattering state around the continuum threshold. Furthermore, we will also investigate CIR [37] in these quasi-low-dimensional systems. Although the main purpose of the paper is to discuss effects induced by SOC, we believe that it would be beneficial to include a reasonable amount of details for the case without SOC. These details not only provide a proper context for the ensuing discussions on systems with SOC but also help to clarify the role of SOC in the two-body problems under review.

2.1 Quasi-one dimension

2.1.1 Bound states

First, we introduce a general formalism to solve for the two-body bound state of two interacting atoms within a quasi-d-dimensional trapping potential with $d = 1$ or 2 [27]. Within the standard two-channel model, the short-range interaction between Feshbach molecules in the closed channel and atoms in the open channel can be modeled by a delta function. The Hamiltonian thus takes the form of $H = H_0 + H_I$, with [43]

$$H_0 = \sum_{\sigma=\uparrow,\downarrow} \int \mathrm{d}^3\boldsymbol{r}\, \Psi_\sigma^\dagger \left(-\frac{\hbar^2\nabla^2}{2m} + \frac{1}{2}m\omega^2 \sum_{i=1}^{3-d} x_i^2 \right) \Psi_\sigma + \int \mathrm{d}^3\boldsymbol{r}\, \Phi^\dagger \left(-\frac{\hbar^2\nabla^2}{4m} + m\omega^2 \sum_{i=1}^{3-d} x_i^2 + \bar{\nu}_b \right) \Phi$$

and

$$H_I = \bar{g}_b \int \mathrm{d}^3\boldsymbol{r} \left(\Psi_\uparrow^\dagger \Psi_\downarrow^\dagger \Phi + \mathrm{h.c.} \right) + \bar{U}_b \int \mathrm{d}^3\boldsymbol{r}\, \Psi_\uparrow^\dagger \Psi_\downarrow^\dagger \Psi_\downarrow \Psi_\uparrow. \tag{1}$$

Here, $\Psi_\sigma(\boldsymbol{r})$ is the fermionic field operator for atoms at position $\boldsymbol{r}$, with atomic mass m and spin $\sigma = (\uparrow, \downarrow)$, $\Phi(\boldsymbol{r})$ is the bosonic operator associated with the molecule, $\bar{\nu}_b$ is the bare detuning, $\bar{g}_b$ is the bare atom-molecule coupling constant, and $\bar{U}_b$ is the bare background atomic scattering amplitude, and h.c. stands for Hermitian conjugate [44]. For quasi-one-dimensional systems, the transverse trapping potential with frequencies $\omega = \omega_x = \omega_y$ corresponds to a two-dimensional (2D) harmonic trap within the x-y plane. For the case of quasi-two dimensions, which will be discussed later, the trap is a one-dimensional (1D) harmonic trap with frequency ω.

The bare scattering parameters are related to the physical ones (with subscript p) via the standard renormalization relations [45, 46]

$$\bar{U}_c^{-1} = -\int \frac{\mathrm{d}^3\boldsymbol{k}}{(2\pi)^3} \frac{1}{2\epsilon_{\boldsymbol{k}}}, \quad \Gamma^{-1} = 1 + \frac{\bar{U}_p}{U_c},$$

$$\bar{U}_b = \Gamma \bar{U}_p, \quad \bar{g}_b = \Gamma \bar{g}_p, \quad \bar{\nu}_p = \bar{\nu}_b + \Gamma \frac{\bar{g}_p^2}{\bar{U}_c}. \tag{2}$$

Here, $\epsilon_{\boldsymbol{k}} = \hbar^2\boldsymbol{k}^2/(2m)$ is the dispersion relation with three-dimensional (3D) momentum $\boldsymbol{k}$, and the integral is taken in three dimensions with an explicit 2D energy cutoff E_c. Hence, $\bar{U}_c^{-1} = m^{3/2}\sqrt{E_c}/2^{3/2}\pi\hbar^3$. The physical parameters $\bar{g}_p$, $\bar{U}_p$, and $\bar{\nu}_p$ can be obtained from the scattering measurements as $\bar{U}_p = 4\pi\hbar^2 a_{bg}/m$, $\bar{g}_p = \sqrt{4\pi\hbar^2\mu_{co}W|a_{bg}|/m}$, and $\bar{\nu}_p = \mu_{co}(B - B_0)$, where μ_{co} is the difference in magnetic moments between the two channels [47]. Here we have assumed that the s-wave scattering length can be written as $a_s = a_{bg}\left[1 - W/(B - B_0)\right]$ near a Feshbach resonance, where a_{bg} is the background scattering length, W is the resonance width, and B_0 is the resonance position.

Since the trapping potential is harmonic in nature, the center-of-mass and the relative degrees of freedom can be separated. By assuming that the center-of-mass degrees of freedom are in the ground mode of the transverse trap, which has zero momentum along the free direction(s), we can rewrite the noninteracting Hamiltonian (in units of $\hbar\omega$) as

$$H_0 = \sum_{\boldsymbol{m}\boldsymbol{k}\sigma} \epsilon_{\boldsymbol{m}\boldsymbol{k}} a_{\boldsymbol{m}\boldsymbol{k}\sigma}^\dagger a_{\boldsymbol{m}\boldsymbol{k}\sigma} + \nu_b b^\dagger b, \tag{3}$$

where $\boldsymbol{m}$ represents the harmonic eigenmodes $\{m_i\}$, $i = 1, \ldots, 3-d$, and $\boldsymbol{k}$ is the plane-wave vector in the untrapped dimensions $\{k_j\}$, $j = 1, \ldots, d$. The operators $a_{\boldsymbol{m}\boldsymbol{k}\sigma}$ and b annihilate the atomic and the molecular modes, respectively. The index of b can be dropped as there is only one molecular mode in the center-of-mass frame. The dimensionless energy $\epsilon_{\boldsymbol{m}\boldsymbol{k}}$ is then given by

$$\epsilon_{\boldsymbol{m}\boldsymbol{k}} = \frac{3-d}{4} + \sum_{i=1}^{3-d} m_i + \frac{a_t^2}{2} \sum_{j=1}^{d} k_j^2, \tag{4}$$

where $a_t = \sqrt{\hbar/m\omega}$ is the trap length scale. Similarly, the interaction Hamiltonian H_I (also in units of $\hbar\omega$) takes the form

$$H_I = \frac{g_b}{a_t^{(3-d)/2} L^{d/2}} \sum_{\boldsymbol{mnk}} \gamma_{\boldsymbol{mn}} \left(a^\dagger_{\boldsymbol{mk}\uparrow} a^\dagger_{\boldsymbol{n-k}\downarrow} b + \text{h.c.} \right) + \frac{U_b}{a_t^{(3-d)} L^d} \sum_{\substack{\boldsymbol{mnk} \\ \boldsymbol{m'n'k'}}} \gamma_{\boldsymbol{mn}} \gamma_{\boldsymbol{m'n'}} a^\dagger_{\boldsymbol{mk}\uparrow} a^\dagger_{\boldsymbol{n-k}\downarrow} a_{\boldsymbol{n'-k'}\downarrow} a_{\boldsymbol{m'k'}\uparrow}, \tag{5}$$

where the coefficients are given by

$$\gamma_{\boldsymbol{mn}} = \prod_{j=1}^{3-d} \begin{cases} \dfrac{(-1)^{(m_j-n_j)/2}}{(2\pi^3)^{1/4}\sqrt{m_j! n_j!}} \Gamma\left(\dfrac{m_j+n_j+1}{2}\right), & m_j + n_j \text{ even}, \\ 0, & m_j + n_j \text{ odd}. \end{cases} \tag{6}$$

Note that, in the expressions above, we use ν_b, g_b, and U_b to denote the corresponding dimensionless parameters in the original Hamiltonian.

A general two-body state of the system can be expressed as [48]

$$|\Psi\rangle = \left(\beta b^\dagger + \sum_{\boldsymbol{mnk}} \eta_{\boldsymbol{mnk}} a^\dagger_{\boldsymbol{mk}\uparrow} a^\dagger_{\boldsymbol{n-k}\downarrow} \right) |0\rangle. \tag{7}$$

By solving the Schrödinger equation $H|\Psi\rangle = E|\Psi\rangle$, we can get the coefficients in the above two-body state:

$$\frac{1}{U_b^{\text{eff}}(E)} = S(E), \tag{8}$$

$$\beta^{-2} = 1 - Z_b^2(E) \frac{\partial S(E)}{\partial E}, \tag{9}$$

$$\eta_{\boldsymbol{mnk}} = \beta \gamma_{\boldsymbol{mn}} (a_t/L)^{d/2} \frac{Z_b(E)}{E - \epsilon_{\boldsymbol{mk}} - \epsilon_{\boldsymbol{nk}}}, \tag{10}$$

where the parameters take the following forms:

$$U_b^{\text{eff}}(E) \equiv U_b - \frac{g_b^2}{\nu_b - E},$$

$$Z_b(E) \equiv g_b - \frac{U_b}{g_b}(\nu_b - E),$$

$$S(E) \equiv \left(\frac{a_t}{L}\right)^d \sum_{\boldsymbol{mnk}} \frac{\gamma_{\boldsymbol{mn}}^2}{E - \epsilon_{\boldsymbol{mk}} - \epsilon_{\boldsymbol{nk}}}.$$

By employing the renormalization relation given by Eq. (2), the parameters listed above can be related to the physical parameters by

$$Z_p(E) \equiv g_p - \frac{U_p}{g_p}(\nu_p - E) = Z_b(E),$$

$$\left[U_p^{\text{eff}}(E)\right]^{-1} \equiv \left(U_p - \frac{g_p^2}{\nu_p - E} \right)^{-1}$$

$$= \left[U_b^{\text{eff}}(E)\right]^{-1} - \bar{U}_c^{-1} a_t^3 \hbar\omega. \tag{11}$$

Notice that the divergence of $\bar{U}_c^{-1}$ exactly cancels the divergence in $S(E)$. Thus, we can rewrite Eq. (8) as

$$\frac{1}{U_p^{\text{eff}}(E)} = S_p(E), \tag{12}$$

where $S_p(E) \equiv S(E) - \bar{U}_c^{-1}$ takes the following form:

$$S_p(E) = \frac{-1}{2^{5/2}\pi} \times \begin{cases} \zeta(1/2, 1/2 - E/2), & d = 1, \\ \displaystyle\int_0^\infty \mathrm{d}s \left(\frac{\Gamma\left(s + \frac{1}{4} - \frac{E}{2}\right)}{\Gamma\left(s + \frac{3}{4} - \frac{E}{2}\right)} - \frac{1}{\sqrt{s}} \right), & d = 2. \end{cases} \tag{13}$$

In the expression above,

$$\zeta(s, x) = \lim_{N\to\infty} \sum_{n=0}^{N} (n+x)^{-s} - \frac{(N+x)^{-s+1}}{-s+1} \tag{14}$$

is the Hurwitz zeta function.

The two-body bound-state energy E can then be determined by solving Eq. (12), while the corresponding wave function can be obtained from Eqs. (9) and (10). In Fig. 1, we show the fractions of the molecular state $|\beta|^2$ and the atomic harmonic eigenstates $P_{\boldsymbol{mn}} = \sum_{\boldsymbol{k}} |\eta_{\boldsymbol{mnk}}|^2$ for the two-body bound state across a wide Feshbach resonance. In this plot, we consider as an example the case of ^{40}K, where the parameters are taken as $W \simeq 8$ G, $a_{bg} \simeq 174 a_B$, and $\mu_{co} \simeq 1.68\mu_B$ with a_B the Bohr radius and μ_B the Bohr magneton [49]. It can be clearly seen that, as the magnetic field is tuned around the resonance point and on the Bose–Einstein condensate (BEC) side of the resonance, the atoms significantly populate the higher harmonic eigenmodes. This can be understood by noticing that, within these regimes, the binding energy of the two-body bound state becomes comparable or even exceeds the transverse

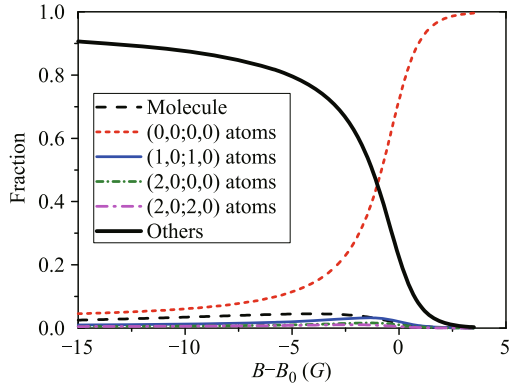

Fig. 1 Population fraction of the two-body bound state in different transverse harmonic levels for ^{40}K in a quasi-1D confinement. Reproduced from Ref. [26].

harmonic trapping frequency, and therefore it can excite the relative motion within the dimer state to higher harmonic levels.

2.1.2 Scattering states

The low-energy scattering processes of two colliding atoms trapped in a quasi-one-dimensional potential were first discussed by Olshanii [37]. In this seminal paper, Olshanii considered the problem in which two atoms are confined in the x-y plane within an axially symmetric 2D harmonic potential of frequency $\omega_\perp = \omega_x = \omega_y$. Along the z direction, the atoms can move freely. The interaction between the two atoms is modeled by the 3D Huang-Yang pseudopotential [50]

$$U(r) = g'\delta(\boldsymbol{r})\frac{\partial}{\partial r}(r\cdot), \tag{15}$$

where $g' = 2\pi\hbar^2 a_s/\mu$ is the interaction strength, and $\mu = m/2$ is the reduced mass.

By separating the center-of-mass and the relative motions in the harmonic potential, we obtain the Schrödinger equation associated with the relative degrees of freedom,

$$\left[\frac{\hat{p}_z^2}{2\mu} + g'\delta(\boldsymbol{r})\frac{\partial}{\partial r}(r\cdot) + \hat{H}_\perp(\hat{p}_x,\hat{p}_y,x,y)\right]\Psi = E\Psi, \tag{16}$$

where $\boldsymbol{r} = \boldsymbol{r}_2 - \boldsymbol{r}_1$ is the relative coordinate between the two atoms and

$$\hat{H}_\perp = \frac{\hat{p}_x^2+\hat{p}_y^2}{2\mu} + \frac{\mu\omega_\perp^2(x^2+y^2)}{2} \tag{17}$$

is the 2D harmonic oscillator Hamiltonian.

Since the interaction is of short range, the asymptotic form of the scattering wave function Ψ can be obtained by solving the noninteracting Hamiltonian, leading to

$$\Psi(z,\rho) \overset{|z|\to\infty}{\longrightarrow} [\mathrm{e}^{\mathrm{i}k_z z} + f_{\mathrm{even}}\mathrm{e}^{\mathrm{i}k_z|z|} + f_{\mathrm{odd}}\,\mathrm{sign}(z)\mathrm{e}^{\mathrm{i}k_z|z|}]\,\phi_{0,0}(\rho), \tag{18}$$

where $\rho = \sqrt{x^2+y^2}$. The first term on the right-hand side of Eq. (18) corresponds to the incident wave, and the second and third terms are, respectively, the even and odd scattered waves with corresponding 1D scattering amplitudes $f_{\mathrm{even}}(k_z)$ and $f_{\mathrm{odd}}(k_z)$. Notice that, by writing Eq. (18), we assume *a priori* that the incident energy is much lower than the transverse trapping frequency with

$$E \equiv \frac{\hbar^2 k_z^2}{2\mu} < E_{n=2,m_z=0} - E_{n=0,m_z=0} = 2\hbar\omega_\perp, \tag{19}$$

so that the incident state and the asymptotic scattered state are frozen at the 2D harmonic ground state $\phi_{n=0,m_z=0}(\rho)$. Here, $E_{n,m_z} = \hbar\omega_\perp(n+1)$ is the energy spectrum of the 2D harmonic oscillator, $n = 0,1,2,\ldots,\infty$ is the principal quantum number, and $m_z = 0,2,4,\ldots,n$ $(1,3,5,\ldots,n)$ is the magnetic quantum number with respect to the z axis for n even (odd).

By substituting the ansatz wave function Eq. (18) into Eq. (16) and applying the continuity conditions at $r = 0$, we obtain the following results for the scattering amplitudes:

$$f_{\mathrm{even}} = -\frac{\mathrm{i}\mu}{\hbar^2 k_z}\phi_{0,0}^*(0)g'\eta', \tag{20}$$

$$f_{\mathrm{odd}} = 0, \tag{21}$$

where

$$\eta' = \frac{\partial}{\partial r}[r\ \Psi(\boldsymbol{r})]\Big|_{r\to 0} = \frac{\partial}{\partial z}[z\ \Psi(z,\rho=0)]\Big|_{z\to 0+}. \tag{22}$$

The expression for the wave function reads

$$\Psi(z,\rho=0) = \frac{1}{\sqrt{\pi}a_\perp}\exp(\mathrm{i}k_z z) - \frac{\mathrm{i}g'\mu\eta'}{\pi\hbar^2 k_z a_\perp^2}\exp(\mathrm{i}k_z|z|) - \frac{g'\mu\eta'}{2\pi\hbar^2 a_\perp}\Lambda\left[\frac{2|z|}{a_\perp}, -\left(\frac{k_z a_\perp}{2}\right)^2\right], \tag{23}$$

where $\Lambda[\xi,\epsilon] = \sum_{s'=1}^{\infty}\exp(-\sqrt{s'+\epsilon}\,\xi)/\sqrt{s'+\epsilon}$ and $a_\perp = [\hbar/(\mu\omega_\perp)]^{1/2}$ is the characteristic length of the ground state of transverse Hamiltonian Eq. (17). To obtain the expression above, we have used the relation $|\phi_{n,m_z=0}(\rho=0)|^2 = 1/\pi a_\perp^2$ for the wave functions of the 2D harmonic oscillator and assumed the value of $\phi_{0,0}(\rho=0)$ to be real and positive without loss of generality.

The parameter η' can be determined from Eq. (22) by using the expansion form of the function $\Lambda[\xi,\epsilon] = 2/\xi + \mathcal{L}(\epsilon) + \mathcal{L}_1(\epsilon)\xi + \ldots$, where $\mathcal{L}(\epsilon) = -\mathcal{C} + \bar{\mathcal{L}}(\epsilon)$ and

$$\mathcal{C} = \lim_{s\to\infty}\left(\int_0^s \frac{d\,s'}{\sqrt{s'}} - \sum_{s'=1}^{s}\frac{1}{\sqrt{s'}}\right) \approx 1.4603, \tag{24}$$

$$\bar{\mathcal{L}}(\epsilon) = \sum_{n=1}^{\infty}(-1)^n\frac{\zeta[(1+2n)/2](2n-1)!!\,\epsilon^n}{2^n n!}, \tag{25}$$

with $\zeta[\xi]$ the Riemann zeta function. Here, we have employed the identity

$$\sum_{s'=1}^{\infty}\int_{s'-1}^{s'} \mathrm{d}s''\,\exp(-\sqrt{s''}\xi)/\sqrt{s''} = 2/\xi. \tag{26}$$

The final expression for the 1D scattering amplitude is

$$f_{\rm even}(k_z) = -\frac{1}{1+{\rm i}k_z a_{\rm 1D} - \underbrace{({\rm i}k_z a_\perp/2)\,\bar{\mathcal{L}}(-k_z^2 a_\perp^2/4)}_{\mathcal{O}((k_z a_\perp)^3)}} \tag{27}$$

with the 1D scattering length

$$a_{\rm 1D} = -\frac{a_\perp^2}{2a_s}\left(1-\mathcal{C}\frac{a_s}{a_\perp}\right). \tag{28}$$

In the low-energy limit, the scattering amplitude of Eq. (27) can be well approximated as $f^{\delta}_{\rm even}(k_z) = -1/(1+ik_z a_{\rm 1D})$, which is the scattering amplitude associated with a 1D contact potential

$$U_{\rm 1D}(z) = g_{\rm 1D}\delta(z), \tag{29}$$

where

$$g_{\rm 1D} = -\frac{\hbar^2}{\mu\, a_{\rm 1D}} = g'\,|\phi_{0,0}(0)|^2\left(1-\mathcal{C}\frac{a_s}{a_\perp}\right)^{-1} \tag{30}$$

with $|\phi_{0,0}(0)|^2 = 1/\pi a_\perp^2$. In Fig. 2, we show the transmission coefficient $\mathcal{T} = |1+f_{\rm even}+f_{\rm odd}|^2$ calculated using the exact result, Eq. (27), and the 1D δ-potential approximation $f_{\rm even} \approx f^{\delta}_{\rm even}$. Note that $f_{\rm odd} = f^{\delta}_{\rm odd} = 0$. This figure shows that the 1D effective potential given by Eqs. (29) and (30) can reproduce the low-energy scattering properties in the presence of a transverse trap.

2.1.3 *Confinement-induced resonance*

From the results of Eqs. (28) and (30), one can see clearly that, as the 3D s-wave scattering length satisfies $a_s/a_\perp = 1/\mathcal{C}$, the 1D scattering length $a_{\rm 1D}$ approaches zero and the system becomes a strongly interacting gas with $g_{\rm 1D} \to \infty$. This regime is of particular interest as it corresponds to a Tonks–Girardeau (TG) gas [51] of impenetrable bosons with $g_{\rm 1D} \to +\infty$. In this case, as can be seen from Fig. 2, the collision of two atoms leads to total reflection with vanishing transmission coefficient. This scheme is known as confinement-induced resonance [37], where the effective 1D coupling constant can be varied from $-\infty$ to $+\infty$ by changing either the 3D s-wave scattering length or the transverse trapping potential.

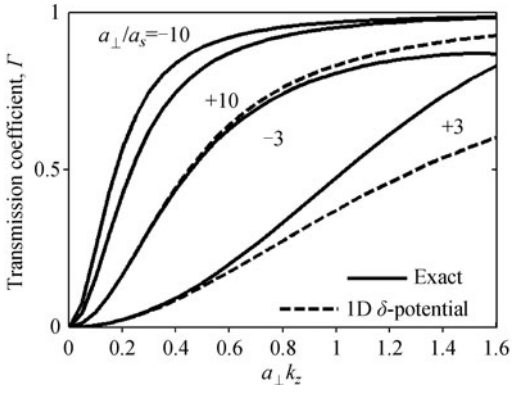

Fig. 2 Transmission coefficient as a function of the incident momentum k_z for different $a_\perp/a_s$. Solid lines correspond to the exact 1D scattering amplitude calculated from Eq. (27). Dashed lines correspond to the 1D δ-potential approximation $f_{\rm even} \approx f^{\delta}_{\rm even}$. Reproduced from Ref. [37].

The underlying physics of CIR can be understood from the perspective of a Feshbach resonance [31, 52–54], where the binding energy of a bound state in the closed channel becomes degenerate with the threshold of the open channel [38]. In the presence of transverse confinement, the scattering of atoms in the transverse ground state assumes the role of an open channel, whereas the transverse excited states serve as the closed channel, which can support a bound state [55].

2.2 Quasi-two dimensions

2.2.1 *Bound states*

Now we proceed to the discussion of two-body physics in a quasi-two-dimensional system. In experiments, a quasi-2D gas can be achieved by applying a strong confinement along the axial (z) direction and a weak harmonic trapping potential in the transverse (x–y) plane [56]. The formalism for the bound state in this system has been introduced in Section 2.1.1; here we should set $d = 2$ and $\omega = \omega_z$.

In Fig. 3, we show as an example the population distribution in transverse levels as functions of the magnetic-field detuning for ^{40}K in a quasi-2D trap. The population fraction in the transverse states $(\boldsymbol{m};\boldsymbol{n})$ is $P_{\boldsymbol{mn}} = \sum_{\boldsymbol{k}} |\eta_{\boldsymbol{mnk}}|^2$. The fraction of the excited states in the transverse direction is $P_{ex} \equiv 1-\beta^2-\sum_k \eta^2_{00k}$. Notice from the results that atoms trapped in quasi-two dimensions cannot be considered to only occupy the transverse

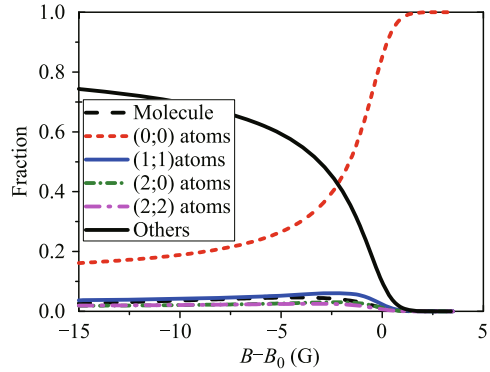

Fig. 3 Population fraction of the two-body bound state in different axial harmonic levels for ^{40}K in a quasi-2D confinement. Reproduced from Ref. [26].

ground level, since a significant fraction of the atomic population resides in the excited transverse levels in the crossover region. This observation is qualitatively consistent with the outcome from the quasi-1D case.

2.2.2 Scattering states

We now turn to the two-body scattering states in quasi-two dimensions. By separating the center-of-mass and relative degrees of freedom, the relative motion is determined by the interatomic interaction potential $V(r)$ and the trapping potential $V_H(z) = m\omega_z^2 z^2/4$, which comes from the tight harmonic confinement along the z axis. By using zeroth-order perturbation theory as in the 3D case [57], the 2D effective coupling constant is given by [58]

$$g = f(E) = \int \mathrm{d}\boldsymbol{r}\psi(\boldsymbol{r})V(r)\psi_f^*(\boldsymbol{r}). \tag{31}$$

The wave function $\psi(\boldsymbol{r})$ of the relative motion of two atoms satisfies the Schrödinger equation

$$\left[-\frac{\hbar^2}{m}\Delta + V(\boldsymbol{r}) + V_H(z) - \frac{\hbar\omega_z}{2}\right]\psi(\boldsymbol{r}) = E\psi(\boldsymbol{r}). \tag{32}$$

The wave function $\psi_f(\boldsymbol{r}) = \varphi_0(z)\exp(\mathrm{i}\boldsymbol{q}\cdot\boldsymbol{\rho})$ describes the free motion in the x–y plane, where $\varphi_0(z)$ is the ground-state wave function of the potential $V_H(z)$, $\boldsymbol{\rho} = \{x, y\}$ and $\boldsymbol{q} = \{q_x, q_y\}$ label 2D coordinates and momentum, respectively, and $q = (2mE/\hbar^2)^{1/2}$. In the weakly interacting regime of $[mg/(2\pi\hbar^2)] \ll 1$, it is possible to use perturbation theory to higher orders [59].

We focus on the case of short-range interaction with $R_e \ll a_z$, where R_e is the characteristic radius of the interaction potential $V(r)$ and $a_z = \sqrt{\hbar/m\omega_z}$. In this limit, the relative motion of atoms is not influenced by the tight confinement, and $\psi(\boldsymbol{r})$ in Eq. (31) can be written as

$$\psi(r) = \eta''\varphi_0(0)\psi_{3\mathrm{D}}(r) \tag{33}$$

with $\psi_{3\mathrm{D}}(r)$ the 3D wave function. In the short-distance regime where $R_e \ll r \ll a_z$, Eq. (33) takes the asymptotic form $\psi = \psi_{\mathrm{as}}(r) = \eta''\varphi_0(0)(1 - a_s/r)$. This expression sets the Bethe-Peierls boundary condition at $r \to 0$ for the solution of Eq. (32) with $V(r) = 0$. Thus, the wave function $\psi(\boldsymbol{r})$ can be obtained with the aid of Green's function $G(\boldsymbol{r}, \boldsymbol{r}')$ as

$$\psi(\boldsymbol{r}) = \varphi_0(z)\exp(\mathrm{i}\boldsymbol{q}\cdot\boldsymbol{\rho}) + AG(\boldsymbol{r}, 0). \tag{34}$$

The coefficients A and η'' can be determined by comparing the solution of Eq. (34) at $r \to 0$ with $\psi_{\mathrm{as}}(r)$.

Using a similar treatment as in the discussion of a purely 1D harmonic oscillator [60], we obtain the Green's function

$$G(\boldsymbol{r}, 0) = \frac{1}{a_z}\int_0^\infty \mathrm{d}t \times \frac{\exp\left[\mathrm{i}\left(\frac{z^2\cot t}{4a_z^2} - q^2a_z^2t - \frac{t}{2} + \frac{\rho^2}{4ta_z^2}\right)\right]}{t\sqrt{(4\pi\mathrm{i})^3\sin t}}. \tag{35}$$

By considering the low-energy condition $qa_z \ll 1$, the expression above can then be reduced to the following form in the limit of $r \ll a_z$:

$$G \approx \frac{1}{4\pi r} + \frac{1}{2(2\pi)^{3/2}a_z}\left[\log\left(\frac{1}{\pi q^2a_z^2}\right) + \mathrm{i}\pi\right]. \tag{36}$$

By omitting the imaginary part of G, we obtain the result for η'' as

$$\eta'' = -\frac{A}{4\pi a_s\varphi_0(0)} = \left(1 + \frac{a_s}{\sqrt{2\pi}a_z}\log\frac{1}{\pi q^2a_z^2}\right)^{-1}. \tag{37}$$

Here, we have used the result $\psi_f = \varphi_0(0) = (1/2\pi a_z^2)^{1/4}$ for the ground harmonic oscillator. By employing the relation $\int \mathrm{d}\boldsymbol{r}\psi_{3\mathrm{D}}(r)V(r) = 4\pi\hbar^2a_s/m$ along with Eqs. (31), (33), and (37), we find the coupling constant

$$g = \frac{2\sqrt{2\pi}\hbar^2}{m}\frac{1}{a_z/a_s + (1/\sqrt{2\pi})\log(1/\pi q^2a_z^2)}. \tag{38}$$

Equation (38) shows that the 2D effective coupling constant g depends on the incident momentum $q = (2mE/\hbar^2)^{1/2}$ and the axial trapping potential in quasi-two dimensions. In the limiting case of $a_z \gg a_s$, the logarithmic term in Eq. (38) can be neglected, and g recovers the 3D form, which is proportional to a_s. Hence, the quasi-2D gas behaves like a 3D system, as one should naturally expect. Another important observation one can extract from Eq. (38) is that the 2D effective coupling constant will diverge as the denominator becomes zero. In the low-energy limit with $qa_z \ll 1$, this quasi-2D confinement-induced resonance takes place on the Bardeen–Cooper–Schrieffer (BCS) side of the Feshbach resonance with $a_s < 0$. This is in clear contrast to the quasi-1D case as discussed in Section 2.1.3, where CIR takes place on the BEC side of the Feshbach resonance.

2.2.3 Confinement-induced resonance

In this subsection, we investigate CIR in the presence of an anisotropic transverse confinement $\omega_x \neq \omega_y$ with the parameter $\eta \equiv \omega_x/\omega_y$. With continuously increasing η, the quasi-1D geometry should eventually cross over to a quasi-2D system [61].

When considering the transverse anisotropy, the Hamiltonian in Eq. (16) introduced in Section 2.1.2 can

be rewritten as

$$\hat{H}_{\rm rel} = -\frac{1}{2}\nabla_{\boldsymbol{r}}^2 + \frac{1}{2}(\eta^2 x^2 + y^2) + 2\pi a_s \delta(\boldsymbol{r})\frac{\partial}{\partial r}(r\cdot). \quad (39)$$

where we set the unit of length as $a_y = \sqrt{\hbar/(\mu\omega_y)}$ and the unit of energy as $\hbar\omega_y$. In Section 2.1.3, we showed that CIR can be regarded as a Feshbach resonance, where the scattering of atoms in the transverse ground state acts as the open channel and the transverse excited states serve as the closed channel. CIR takes place when bound states in the closed channel become degenerate with the continuum threshold of the open channel. We now adopt this picture and study the bound states of the closed channel and examine the CIR condition from the binding energy.

To facilitate derivation, we impose a very shallow harmonic potential along the z direction with a trapping frequency $\omega_z = \epsilon\omega_y$, so that we always have a well-defined two-body bound state. The case of free-collision along the z direction hence corresponds to the limiting case of $\epsilon \to 0$. The dimensionless relative Hamiltonian takes the following form:

$$\hat{H}'_{\rm rel} = -\frac{1}{2}\nabla_{\boldsymbol{r}}^2 + \frac{1}{2}(\eta^2 x^2 + y^2 + \epsilon^2 z^2) + 2\pi a_s \delta(\boldsymbol{r})\frac{\partial}{\partial r}(r\cdot). \quad (40)$$

Then we split the Hamiltonian into "ground" (g), "excited" (e), and "ground-excited coupling" (ge) parts:

$$\begin{aligned}\hat{H}'_{\rm rel} &= \hat{H}_g + \hat{H}_e + \hat{H}_{ge} \\ &= \hat{P}_g\hat{H}\hat{P}_g + \hat{P}_e\hat{H}\hat{P}_e + (\hat{P}_g\hat{H}\hat{P}_e + \hat{P}_e\hat{H}\hat{P}_g), \end{aligned} \quad (41)$$

where $\hat{P}_g = |00\rangle_\perp\langle 00|$, $\hat{P}_e = \sum_{(n_x,n_y)'} |n_x n_y\rangle_\perp\langle n_x n_y|$ are the projection operators, $|n_x n_y\rangle_\perp$ is the eigenstate of the transverse harmonic oscillators with quantum numbers n_x and n_y, and the summation $(n_x, n_y)'$ runs over all possible combinations except the ground mode $|00\rangle_\perp$.

In the limit of $\epsilon \to 0$, the spectrum of $\hat{H}_g$ is continuous for energies above the threshold energy $E_{g0} = (\eta+1)/2$, which is also the zero-point energy of the transverse mode. The spectrum of $\hat{H}_e$ is also continuous for energies higher than $E_{e0} = 3(\eta+1)/2$. However, as we will become evident below, $\hat{H}_e$ supports a bound state with energy $E_{eb} < E_{e0}$ for all values of the 3D scattering length a_s. Hence, CIR would take place when the bound-state energy of $\hat{H}_e$ is degenerate with the continuum threshold of $\hat{H}_g$, leading to the resonance condition

$$E_{eb} = E_{g0} = \frac{\eta+1}{2}. \quad (42)$$

To find E_{eb}, we project the total wave function Ψ onto the excited Hilbert space $\Psi_e = \hat{P}_e\Psi$, and rewrite the

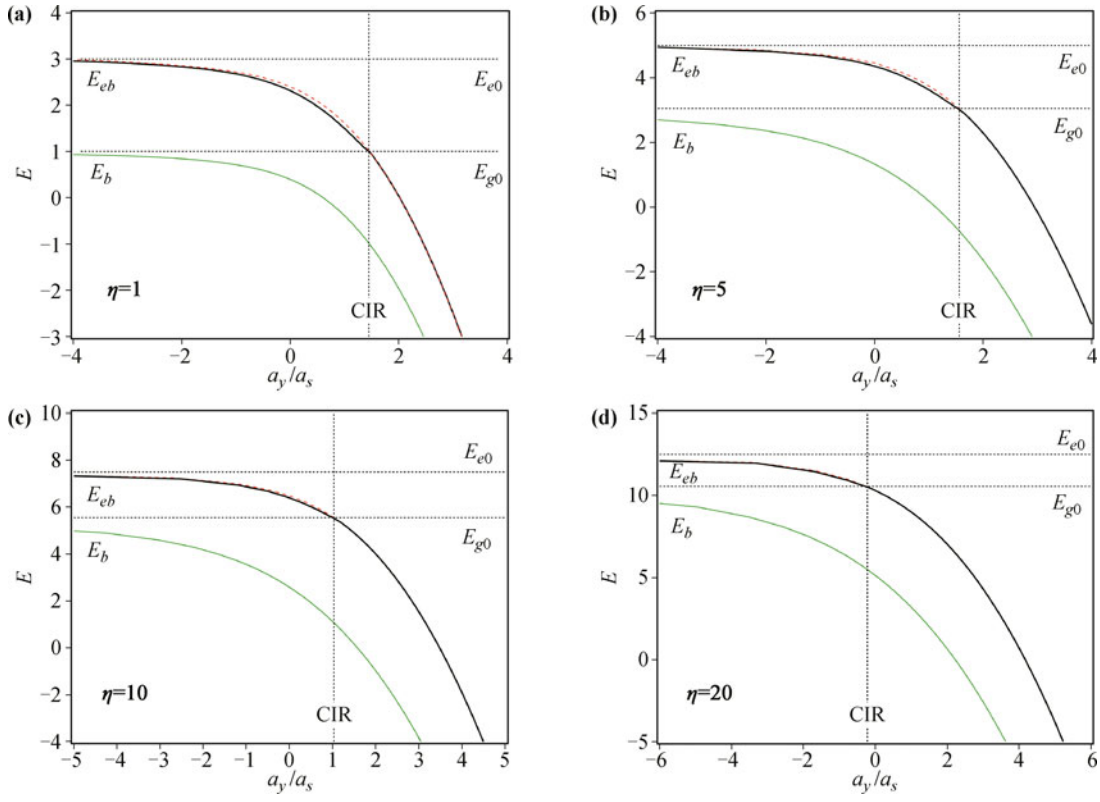

Fig. 4 Bound-state energy E_{eb} within the closed-channel and the bound-state energy E_b of the full Hamiltonian. The solid lines are calculated with the limit $\epsilon = \omega_z/\omega_y \to 0$, and the dashed lines correspond to the results for $\epsilon = 0.1$. The crossing point between E_{eb} and E_{g0} indicates the position of CIR. Reproduced from Ref. [61].

wave function as [39]

$$\Psi_e(\boldsymbol{r}) = \sum_{(n_x,n_y)'} \sum_{n_z} c_{n_x n_y n_z} \Phi_{n_x}(\sqrt{\eta}x)\Phi_{n_y}(y)\Phi_{n_z}(\sqrt{\epsilon}z), \tag{43}$$

where

$$\Phi_n(t) = \frac{\mathrm{e}^{-t^2/2}}{\pi^{1/4}\sqrt{2^n n!}} H_n(t). \tag{44}$$

Here, $H_n(t)$ is the Hermite polynomial. Substituting the expansion of Eq. (43) into the Schrödinger equation $\hat{H}\,\Psi_e = E\,\Psi_e$, we have

$$\begin{aligned} 0 = &\sum_{(n_x,n_y)'} \sum_{n_z} c_{\boldsymbol{n}}(E_{\boldsymbol{n}} - E)\mathcal{P}_{\boldsymbol{n}}(x,y,z) \\ &+2\pi a_s \delta(\boldsymbol{r})\frac{\partial}{\partial r} r \sum_{(n_x,n_y)'} \sum_{n_z} c_{\boldsymbol{n}}\mathcal{P}_{\boldsymbol{n}}(x,y,z), \end{aligned} \tag{45}$$

with

$$\mathcal{P}_{\boldsymbol{n}}(x,y,z) \equiv \Phi_{n_x}(\sqrt{\eta}x)\Phi_{n_y}(y)\Phi_{n_z}(\sqrt{\epsilon}z). \tag{46}$$

Here, $\boldsymbol{n}$ represents (n_x, n_y, n_z), and $E_{\boldsymbol{n}} = (n_x + 1/2)\eta + (n_y+1/2)+(n_z+1/2)\epsilon$ is the eigenenergy of 3D harmonic oscillator. Projecting Eq. (45) onto state $\Phi_{n'_x}\Phi_{n'_y}\Phi_{n'_z}$ with arbitrary n'_x, n'_y, and n'_z, we obtain

$$c_{\boldsymbol{n}} = \frac{2\pi a_s\sqrt{\eta\epsilon}\mathcal{P}_{\boldsymbol{n}}(0,0,0)\mathcal{C}}{E - E_{\boldsymbol{n}}}. \tag{47}$$

Here the value of $\mathcal{C}$ is related to

$$\mathcal{C} = \left[\frac{\partial}{\partial r} r\,\Psi_e(\boldsymbol{r})\right]_{r\to 0}. \tag{48}$$

Substituting Eq. (47) into (48), we can get the equation for the the eigenenergy E,

$$-\frac{1}{2\pi a_s} = \left[\frac{\partial}{\partial r} r\,\Psi_e(\mathcal{E},\boldsymbol{r})\right]_{r\to 0}, \tag{49}$$

where

$$\Psi_e(\mathcal{E},\boldsymbol{r}) = \sum_{(n_x,n_y)'} \sum_{n_z} \frac{\sqrt{\eta\epsilon}\mathcal{P}_{\boldsymbol{n}}(0,0,0)\mathcal{P}_{\boldsymbol{n}}(x,y,z)}{n_x\eta + n_y + n_z\epsilon - \mathcal{E}}, \tag{50}$$

and $\mathcal{E} = E - E_0$ is the energy shifted by the zero-point energy $E_0 = (\eta + 1 + \epsilon)/2$.

By applying the generating function for the products of Hermite polynomials [62],

$$\sum_{n=0}^{\infty} \frac{\sigma^n}{2^n n!} H_n(x)H_n(y) = \frac{\mathrm{e}^{(2\sigma xy - \sigma^2x^2 - \sigma^2y^2)/(1-\sigma^2)}}{\sqrt{1-\sigma^2}}, \tag{51}$$

and the identity [63]

$$\frac{1}{n_x\eta + n_y + n_z\epsilon - \mathcal{E}} = \int_0^\infty \mathrm{d}t \mathrm{e}^{-t(n_x\eta + n_y + n_z\epsilon - \mathcal{E})}, \tag{52}$$

we can get the wave function

$$\Psi_e(\mathcal{E},\boldsymbol{r}) = \psi_e^{\mathrm{I}}(\mathcal{E},\boldsymbol{r}) + \psi_e^{\mathrm{II}}(\mathcal{E},\boldsymbol{r}), \tag{53}$$

where

$$\begin{aligned} \psi_e^{\mathrm{I}}(\mathcal{E},\boldsymbol{r}) &= \frac{\sqrt{\eta\epsilon}}{(2\pi)^{3/2}} \int_0^\infty \mathrm{d}t \frac{\mathrm{e}^{t(\mathcal{E}+E_0)}}{\sqrt{\sinh(\eta t)\sinh(t)\sinh(\epsilon t)}} \\ &\quad\times \exp\left[-\frac{\eta x^2}{2}\coth(\eta t) - \frac{y^2}{2}\coth(t) - \frac{\epsilon z^2}{2}\coth(\epsilon t)\right], \\ \psi_e^{\mathrm{II}}(\mathcal{E},\boldsymbol{r}) &= \frac{-2\sqrt{\eta\epsilon}}{(2\pi)^{3/2}} \int_0^\infty \mathrm{d}t \frac{1}{\sqrt{\sinh(t)}} \\ &\quad\times \exp\left[t\left(\mathcal{E} + \frac{\epsilon}{2}\right) - \frac{\eta x^2 + y^2}{2} - \frac{\epsilon z^2}{2}\coth(\epsilon t)\right]. \end{aligned} \tag{54}$$

Note that the integral of ψ_e^{II} is well behaved at $r = 0$:

$$\begin{aligned} \psi_e^{\mathrm{II}}(\mathcal{E}, r=0) &= -\frac{\sqrt{\eta\epsilon}}{\pi^{3/2}} \int_0^\infty \mathrm{d}t \frac{\mathrm{e}^{t\mathcal{E}}}{\sqrt{1-\mathrm{e}^{-2\epsilon t}}} \\ &= -\frac{\sqrt{\eta}}{2\pi\sqrt{\epsilon}} \frac{\Gamma(-\mathcal{E}/2\epsilon)}{\Gamma(-\mathcal{E}/2\epsilon + 1/2)}, \end{aligned} \tag{55}$$

while ψ_e^{I} is divergent in the limit of $r \to 0$, where the main contribution to the integral comes from the region of small t:

$$\psi_e^{\mathrm{I}}(\mathcal{E},\boldsymbol{r}) \approx \frac{1}{(2\pi)^{3/2}} \int_0^\infty \mathrm{d}t \frac{\mathrm{e}^{-r^2/(2t)}}{t^{3/2}} = \frac{1}{2\pi r}. \tag{56}$$

Substituting the expression of Eq. (53) for the wave function Ψ_e into Eq. (49), we may regularize the divergent behavior with the operator $\partial_r(r\cdot)$. Therefore, we can subtract the right-hand side of Eq. (56) from Ψ_e and obtain a simpler expression for the bound-state energy:

$$\frac{-\sqrt{\pi}}{a_s} = \mathcal{F}(\mathcal{E}), \tag{57}$$

where

$$\begin{aligned} \mathcal{F}(\mathcal{E}) = \int_0^\infty \mathrm{d}t \Bigg[&\frac{\sqrt{\eta\epsilon}\mathrm{e}^{t\mathcal{E}/2}}{\sqrt{(1-\mathrm{e}^{-\eta t})(1-\mathrm{e}^{-t})(1-\mathrm{e}^{-\epsilon t})}} \\ &- \frac{\sqrt{\eta\epsilon}\mathrm{e}^{t\mathcal{E}/2}}{\sqrt{1-\mathrm{e}^{-\epsilon t}}} - \frac{1}{t^{3/2}}\Bigg]. \end{aligned} \tag{58}$$

We can use this equation for all values of $\mathcal{E} \leqslant 0$. When $\mathcal{E} = 0$, the second and third terms eliminate the divergence for $t \to \infty$ and $t \to 0$, respectively, leading to a convergent result of $\mathcal{F}(0)$. By considering the condition that CIR takes place when the eigenenergy $E_{eb} = \mathcal{E} + E_0 = E_{g0}$, we can arrive at the equation for the CIR condition (in physical units):

$$\frac{a_s}{a_y} = -\frac{\sqrt{\pi}}{\mathcal{F}(0)}. \tag{59}$$

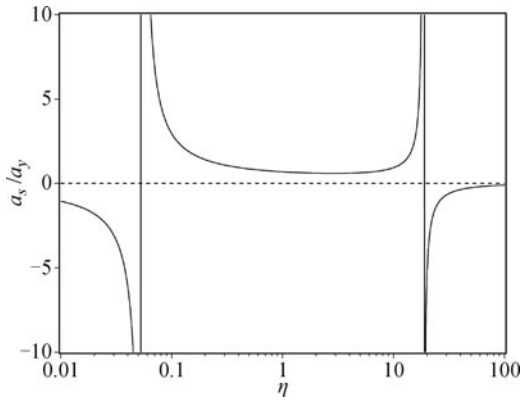

Fig. 5 Locations of CIR versus the parameter $\eta = \omega_x/\omega_y$ describing the transverse anisotropy. Reproduced from Ref. [61].

In Fig. 4, we show that the bound-state energy E_{eb} in the closed channel changes with the 3D scattering length a_s/a_y for several different values of η. In each plot, the location of CIR is found when the energy E_{eb} goes across the open-channel threshold E_{g0}. When considering the quasi-1D system, we should set $\epsilon = \omega_z/\omega_y$ as an infinitesimally small value. However, from our calculation, we find that the quasi-1D regime is already realized for $\epsilon \sim 0.1$, which is shown as the dashed lines in Fig. 4.

The locations of CIR for a wide range of η are shown in Fig. 5. Notice that the resonance position of a_s/a_y changes nonmonotonically with η and diverges at $\eta_c \approx 18.0$, where the 3D scattering length goes through the Feshbach resonance toward the BCS side. As mentioned above, by continuously increasing η, the quasi-1D geometry will eventually cross over to a quasi-2D system, where the s-wave CIR takes place on the BCS side of the Feshbach resonance.

3 Two-body physics in quasi-low dimensions with SOC

In the previous section, we have discussed two-body problems in quasi-one and quasi-two dimensions in the absence of SOC. The analysis therein not only gives a general understanding of the bound and the scattering states in quasi-low-dimensional confinement but also introduces some useful methods to tackle two-body problems. We now turn to the effects caused by SOC.

3.1 Quasi-one dimension

We first investigate two-body problems in a quasi-1D geometry in the presence of the 1D SOC that has been realized at the National Institute of Standards and Technology (NIST) [2]. In the experiment, while the center-of-mass motions of the atoms along a given spatial direction are coupled to the internal spin degrees of freedom, an effective Zeeman field is also implemented simultaneously. For the regime where the energy is close to the threshold, we analyze the effect of SOC and the Zeeman field on the position of CIRs. For energies below the threshold, we give solutions of two-body bound states and confirm that the crossover point of the two-body bound-state energy and the open-channel threshold exactly indicates the position of CIR.

The Hamiltonian for two spin–1/2 atoms with 1D SOC in a quasi-1D configuration is

$$\hat{H}_0 = -\frac{\hbar^2}{2m}\left(\nabla^2_{\boldsymbol{r}_1} + \nabla^2_{\boldsymbol{r}_2}\right) + U(\boldsymbol{r}_1) + U(\boldsymbol{r}_2) + \hat{H}^1_{\rm SOC} + \hat{H}^2_{\rm SOC}, \tag{60}$$

where m is the atomic mass, $\boldsymbol{r}_{j=1,2} \equiv (x_j, y_j, z_j)$ denotes the spatial position of the jth atom, and $U(\boldsymbol{r}_j) \equiv m\omega^2(y_j^2 + z_j^2)/2$ is the quasi-1D confinement within the radial y-z plane with trapping frequency $\omega = \omega_y = \omega_z$. The SOC terms take the form

$$\hat{H}^j_{\rm SOC} = \lambda p_x^{(j)}\sigma_x^{(j)} + h\sigma_z^{(j)} + h_x\sigma_x^{(j)}, \tag{61}$$

where $p_x^{(j)}$ is the linear momentum along the x axis of the jth atom, $\sigma_i^{(j)}$ are Pauli matrices, λ is the intensity of in-line SOC, and h and h_x are the effective Zeeman fields along the transverse and axial directions, respectively. Since the in-line field h_x is not the key to the topological superfluid phases [64], here we consider the situation where $h_x = 0$ for simplicity. However, we note that all our calculations can be easily expanded to cases with finite h_x.

Because of SOC, we cannot separate the center-of-mass and the relative degrees of freedom along the SOC direction in the two-particle system. Rewriting the quantum state of relative degrees of freedom with a spinor wave function

$$|\psi(\boldsymbol{r})\rangle = \psi_{\uparrow\uparrow}(\boldsymbol{r})|\uparrow\rangle_1|\uparrow\rangle_2 + \psi_{\uparrow\downarrow}(\boldsymbol{r})|\uparrow\rangle_1|\downarrow\rangle_2 + \psi_{\downarrow\uparrow}(\boldsymbol{r})|\downarrow\rangle_1|\uparrow\rangle_2 + \psi_{\downarrow\downarrow}(\boldsymbol{r})|\downarrow\rangle_1|\downarrow\rangle_2, \tag{62}$$

we can arrange the Hamiltonian of the relative motion along the x axis into the following form:

$$\hat{H}_{\rm rel} = -\sum_{s=x,y,z}\frac{\partial^2}{\partial s^2} + \frac{1}{4}\sum_{s=y,z}(s^2-1) + \lambda\sum_{j=1,2}\left[\frac{Q_x}{2} + (-1)^j k_x\right]\sigma_x^{(j)} + h\sum_{j=1,2}\sigma_z^{(j)}, \tag{63}$$

where k_x is the relative momentum along the x axis. Here, we use the natural units with $\hbar = m = 1$, and set $\omega = 1$ as the energy unit. We also neglect the zero-point energy of the transverse motion along the y and z

directions for simplicity.

To investigate the two-body scattering process in this system, we first define the single-particle spin state of the jth atom as

$$(\lambda k_x \sigma_x^{(j)} + h\sigma_z^{(j)})|\alpha_j, (\lambda k_x, h)\rangle \equiv \alpha_j \sqrt{\lambda^2 k_x^2 + h^2}|\alpha_j, (\lambda k_x, h)\rangle, \tag{64}$$

where $\alpha_j = \pm 1$ denotes the helicity index. Then the two-particle spin state can be defined as

$$|\boldsymbol{\alpha}(k_x)\rangle = |\alpha_1, (\lambda k_x, h)\rangle_1 |\alpha_2, (-\lambda k_x, h)\rangle_2 \tag{65}$$

with $\boldsymbol{\alpha} \equiv (\alpha_1, \alpha_2)$ used as shorthand notation. The incident wave function can thus be written in the following form with the proper symmetry:

$$|\psi_c^{(0)}(\boldsymbol{r})\rangle = \frac{e^{ik_x x}}{2\sqrt{\pi}} \left[|\boldsymbol{\alpha}(k_x)\rangle - |\boldsymbol{\alpha}'(-k_x)\rangle\right] \phi_0(y)\phi_0(z), \tag{66}$$

where ϕ_0 is the ground state of a 1D harmonic oscillator, and $\boldsymbol{\alpha}' \equiv (\alpha_2, \alpha_1)$. We denote the scattering channel by $c = (\boldsymbol{\alpha}, k_x)$. We can directly calculate the eigenenergy corresponding to Eq. (66), which leads to

$$\varepsilon = \varepsilon_c + (m + n), \tag{67}$$

where $\varepsilon_c = k_x^2 + (\alpha_1 + \alpha_2)\sqrt{\lambda^2 k_x^2 + h^2}$. We note that the threshold energy is shifted from zero to a nonzero value because of SOC:

$$\varepsilon_{\rm th} = \begin{cases} -2h, & \lambda^2 < h, \\ -\lambda^2 - h^2/\lambda^2, & \lambda^2 \geqslant h. \end{cases} \tag{68}$$

Since the scattering energy is within the low-energy regime with $\varepsilon_c - \varepsilon_{\rm th} \ll 1/R_e^2$, where R_e is the length scale associated with the interparticle interacting potential, the wave function of the scattering state can be expressed as [41, 65, 66]

$$|\psi_c(\boldsymbol{r})\rangle \approx |\psi_c^{(0)}(\boldsymbol{r})\rangle + \frac{A(c)}{\phi_0(0)^2} G_0(\varepsilon_c; \boldsymbol{r}, \boldsymbol{0})|0, 0\rangle \tag{69}$$

in the asymptotic region of $r \gtrsim R_e$. Here, $A(c)$ is a coefficient that needs to be determined, $G_0(\varepsilon_b; \boldsymbol{r}, \boldsymbol{r}')$ is the Green's function related to the free Hamiltonian that describes the relative motion of the two interacting atoms,

$$G_0(\varrho; \boldsymbol{r}, \boldsymbol{r}') = \frac{1}{\varrho + i0^+ - \hat{H}_{\rm rel}} \delta(\boldsymbol{r} - \boldsymbol{r}'), \tag{70}$$

and $|0, 0\rangle$ represents a spin singlet state.

Similar to the scattering state, when the energy ε_b of the bound state satisfies the relation $\varepsilon_{\rm th} - \varepsilon_b \ll 1/R_e^2$, i.e., ε_b lies close enough to the threshold, the wave function $|\psi_b(\boldsymbol{r})\rangle$ of the two-body bound state can be approximated as

$$|\psi_b(\boldsymbol{r})\rangle \approx B G_0(\varepsilon_b; \boldsymbol{r}, \boldsymbol{0})|0, 0\rangle \tag{71}$$

in the region of $r \gtrsim R_e$, where B is the normalization constant. We can get the coefficients $A(c)$ and B in Eqs. (69) and (71) by implementing the Bethe-Peierls boundary condition:

$$\psi \propto (1/r - 1/a_s), \quad r \to 0. \tag{72}$$

Specifically, using the identity

$$\delta(\boldsymbol{r} - \boldsymbol{r}') = \int_{-\infty}^{\infty} dk_x \frac{e^{ik_x(x - x')}}{2\pi} \left(\sum_{\boldsymbol{\alpha}} |\boldsymbol{\alpha}(k_x)\rangle\langle\boldsymbol{\alpha}(k_x)|\right) \times \left(\sum_{m,n} \phi_m^*(y')\phi_m(y)\phi_n^*(z')\phi_n(z)\right) \tag{73}$$

and the relation

$$\hat{H}_{\rm rel} e^{ik_x x}\phi_m(y)\phi_n(z)|\boldsymbol{\alpha}(k_x)\rangle = (\varepsilon_c + m + n)e^{ik_x x}\phi_m(y)\phi_n(z)|\boldsymbol{\alpha}(k_x)\rangle, \tag{74}$$

where ϕ_m is the mth eigenstate of a one-dimensional harmonic oscillator, we can obtain the behavior of the Green's function $G_0(\varrho; \boldsymbol{r}, \boldsymbol{0})$ at $r \to 0$:

$$\langle 0, 0|G_0(\varrho; \boldsymbol{r}, \boldsymbol{0})|0, 0\rangle = \langle 0, 0|g(\varrho; \boldsymbol{r}, \boldsymbol{0})|0, 0\rangle + \mathcal{S}(\varrho, \boldsymbol{r}). \tag{75}$$

The terms in the equation above are defined as

$$\langle 0, 0|g(\varrho; \boldsymbol{r}, \boldsymbol{0})|0, 0\rangle = \sum_{m,n} \int dk_x \frac{e^{ik_x x}}{2\pi} \frac{1}{\varrho + i0^+ - (k_x^2 + m + n)} \phi_m^*(0)\phi_m(y)\phi_n^*(0)\phi_n(z), \tag{76}$$

$$\mathcal{S}(\varrho, \boldsymbol{r}) = \sum_{\boldsymbol{\alpha}', m, n} \int_{-\infty}^{\infty} dk_x' \frac{e^{ik_x' x}}{2\pi} |\langle 0, 0|\boldsymbol{\alpha}'(k_x')\rangle|^2 \phi_m^*(0)\phi_m(y)\phi_n^*(0)\phi_n(z) \times \left[\frac{1}{\varrho + i0^+ - (\varepsilon_{c'} + m + n)} - \frac{1}{\varrho + i0^+ - (k_x'^2 + m + n)}\right]. \tag{77}$$

The first term of Eq. (75) is the Green's function associated with the relative Hamiltonian without SOC, while the second term is the contribution from SOC. By substituting Eqs. (75)–(77) into Eqs. (69) and (71), we can solve the scattering and bound states under the Bethe-Peierls boundary condition Eq. (72).

Following the procedure outlined above, we can determine the 1D scattering length (in physical units) as

$$a_{1\mathrm{D}} = -\frac{a_t^2}{a_s}\left\{1 - \frac{a_s}{a_t}\left[2\pi\mathcal{S}_s(\varepsilon_c) - \frac{\zeta\left(1/2, 1-\varepsilon_c/2\right)}{\sqrt{2}}\right]\right\}, \tag{78}$$

where $a_t = \sqrt{\hbar/m\omega}$ and $\zeta(s,a)$ is the Hurwitz zeta function.

The CIR indicates complete reflection with $a_{1\mathrm{D}} = 0$. Thus, the position of the resonance can be derived from Eq. (78), which leads to [67]

$$\frac{a_t}{a_s} = 2\pi\mathcal{S}_s(\varepsilon_{\mathrm{th}}) - \frac{\zeta\left[1/2, 1-\varepsilon_{\mathrm{th}}/2\right]}{\sqrt{2}}. \tag{79}$$

In Fig. 6, we show the position of CIR by varying the amplitudes of the effective Zeeman field h and SOC strength λ. As shown in Fig. 6(a), a_t/a_s increases monotonically with the effective Zeeman field when the SOC strength is fixed. In the zero-field limit, as the SOC can then be gauged away via a unitary transformation, the position of the CIR is reduced to $a_t/a_s = \zeta(1/2,1) \approx 1.0326$ for the case without SOC [37]. From Fig. 6(b), we find that a_t/a_s decreases monotonically with increasing SOC intensity when the effective Zeeman field is fixed. We also note that, in the large-SOC limit, the effect of the Zeeman field becomes negligible, so the position of CIR takes the same value $a_t/a_s = \zeta(1/2,1)$ as in the zero-field limit. However, when the strength of SOC tends to zero, the position of CIR approaches a limiting value, and this phenomenon is different from the case without SOC. In fact, because SOC can mix the two spin states, the two-body threshold energy acquires a significant change even if the SOC is infinitesimally small. As a consequence, SOC will lead to a finite shift of the position of CIR.

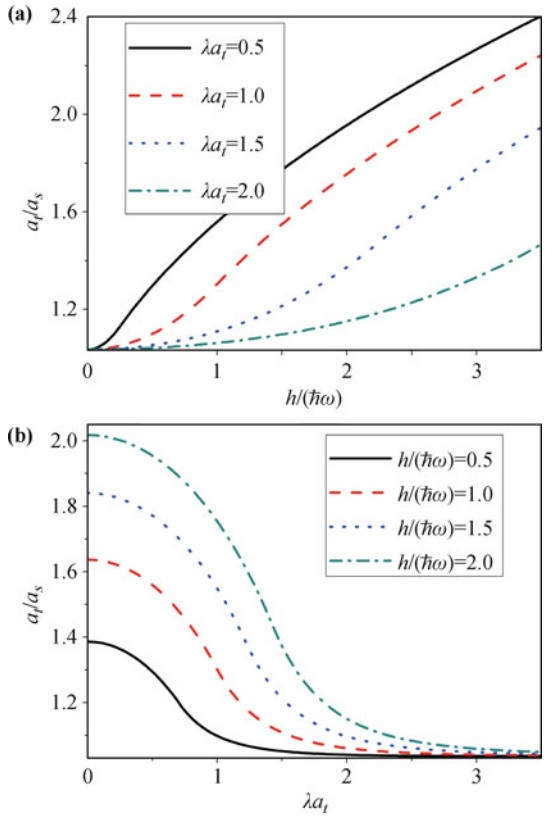

Fig. 6 Position of CIR a_t/a_s versus different **(a)** Zeeman field intensities h and **(b)** SOC strengths λ. Reproduced from Ref. [68].

Similar to the case without SOC, it is also illuminating to consider CIR under SOC as a Feshbach resonance. In the presence of SOC, the two-body bound-state energy ε_e within the closed channel can be calculated via an approach similar to that introduced before, which leads to

$$\frac{1}{a_s} = 2\pi\mathcal{S}_e(\varepsilon_e) - \frac{\zeta\left[1/2, 1-\varepsilon_e/2\right]}{\sqrt{2}}, \tag{80}$$

where the function $\mathcal{S}_e$ takes the form

$$\mathcal{S}_e(\varepsilon_e) = \frac{1}{2\pi}\sum_{s=1}^{\infty}\frac{b}{E_s b + d} \times\left\{\frac{\sqrt{2\gamma - 2E_s - b}\left[2d - b\left(\gamma - E_s\right)\right]}{4E_s b + b^2 + 4d} - \sqrt{-E_s}\right\}. \tag{81}$$

Here, $\gamma = \sqrt{E_s^2 - d}$, $E_s = \varepsilon_e - 2s$, $b = 4\lambda^2$, and $d = 4h^2$. In Fig. 7, we show ε_e as a function of a_t/a_s for various SOC intensities and effective Zeeman field values. From this figure, we confirm once again that the position of CIR exactly corresponds to the crossing point of ε_e and the open-channel threshold $\varepsilon_{\mathrm{th}}$ (denoted by dotted lines in Fig. 7).

3.2 Quasi-two dimensions

Now we turn to a quasi-2D configuration with a harmonic trap with frequency ω_z applied along the z direction, while the atomic motion in the x-y plane is free. The system is subjected to a Rashba-type SOC, with the Hamiltonian describing the atomic relative motion of

$$H = H_0^{(2\mathrm{D})} + H_z + V_{3\mathrm{D}}(r), \tag{82}$$

where $H_0^{(2\mathrm{D})}$ is the 2D free Hamiltonian given by

$$H_0^{(2\mathrm{D})} = -\sum_{\vartheta=x,y}\frac{\partial^2}{\partial\vartheta^2} + \frac{\lambda}{2}\sum_{j=1,2}\left[\frac{q_x}{2} + (-1)^j p_x\right]\hat{\sigma}_x^{(j)} + \frac{\lambda}{2}\sum_{j=1,2}\left[\frac{q_y}{2} + (-1)^j p_y\right]\hat{\sigma}_y^{(j)} \tag{83}$$

with $\boldsymbol{q} = (q_x, q_y)$ the 2D center-of-mass momentum, $\boldsymbol{p} = (p_x, p_y)$ the 2D relative momentum, and λ the

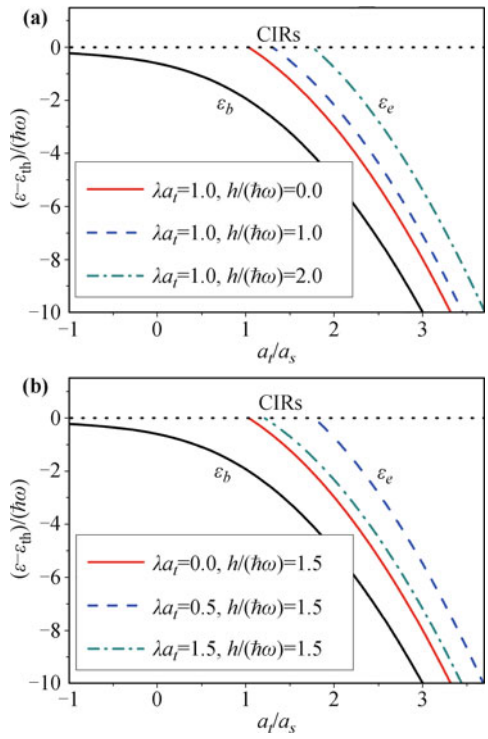

Fig. 7 Two-body bound-state energies ε_b and ε_e versus a_t/a_s for various **(a)** effective Zeeman fields with a given SOC intensity and **(b)** SOC intensities with a given effective Zeeman field. Reproduced from Ref. [68].

SOC intensity. We can define the spin operator $\hat{\sigma}_{x,y}^{(j)}$ for the jth atom as $\hat{\sigma}_x^{(j)} = |\uparrow\rangle_j\langle\downarrow| + |\uparrow\rangle_j\langle\downarrow|$ and $\hat{\sigma}_y^{(j)} = -\mathrm{i}|\uparrow\rangle_j\langle\downarrow| + \mathrm{i}|\downarrow\rangle_j\langle\uparrow|$. We also set the SOC intensity λ in Eq. (83) as a real positive number without loss of generality.

In Eq. (82), the second term on the right-hand side,

$$H_z = -\frac{\partial^2}{\partial z^2} + \frac{\omega_z^2 z^2}{4} - \frac{\omega_z}{2}, \tag{84}$$

is the Hamiltonian describing the relative motion of the atoms in the z direction, where z labels the relative coordinate of the two atoms in this direction. The atom-atom interaction potential $V_{3\mathrm{D}}(r)$ in Eq. (82) changes as a function of the 3D relative coordinate $\boldsymbol{r} = (\boldsymbol{\rho}, z) = (x, y, z)$. Here, we set $r = |\boldsymbol{r}|$ and the effective range of $V_{3\mathrm{D}}(r)$ as r_*. In the region $r \gtrsim r_*$, we can neglect the potential $V_{3\mathrm{D}}(r)$.

First, we consider the scattering state of two atoms residing in the ground state of H_z. The incident wave function can be written as

$$|\Psi_c^{(0)}(\boldsymbol{r})\rangle = \varphi_0(z)\,|\psi_c^{(0)}(\boldsymbol{\rho})\rangle, \tag{85}$$

where $|\psi_c^{(0)}(\boldsymbol{\rho})\rangle$ is an incident wave function in a purely 2D geometry given by

$$|\psi_c^{(0)}(\boldsymbol{\rho})\rangle = \frac{\mathrm{e}^{\mathrm{i}\boldsymbol{k}\cdot\boldsymbol{\rho}}}{2^{3/2}\pi}|\boldsymbol{\alpha}(\boldsymbol{q},\boldsymbol{k})\rangle - \frac{\mathrm{e}^{-\mathrm{i}\boldsymbol{k}\cdot\boldsymbol{\rho}}}{2^{3/2}\pi}|\bar{\boldsymbol{\alpha}}(\boldsymbol{q},-\boldsymbol{k})\rangle. \tag{86}$$

Here, $\boldsymbol{k} = (k_x, k_y)$ is the incident momentum, $\boldsymbol{\rho} = (x, y)$ is the 2D relative coordinate of the two atoms, and $|\boldsymbol{\alpha}(\boldsymbol{q},\boldsymbol{k})\rangle$ is the two-atom spin state defined as

$$|\boldsymbol{\alpha}(\boldsymbol{q},\boldsymbol{k})\rangle = |\alpha_1, \frac{\boldsymbol{q}}{2} + \boldsymbol{k}\rangle_1 |\alpha_2, \frac{\boldsymbol{q}}{2} - \boldsymbol{k}\rangle_2 \tag{87}$$

with $\boldsymbol{\alpha} = (\alpha_1, \alpha_2)$ and $\bar{\boldsymbol{\alpha}} = (\alpha_2, \alpha_1)$. To simplify notations, we denote $c = (\boldsymbol{\alpha}, \boldsymbol{q}, \boldsymbol{k})$ as the set of all three quantum numbers in the following discussion.

With respect to the incident state $|\Psi_c^{(0)}(\boldsymbol{r})\rangle$, the scattering state $|\Psi_c^{(+)}(\boldsymbol{r})\rangle$ in the region of $r \gtrsim r_*$ takes the form

$$|\Psi_c^{(+)}(\boldsymbol{r})\rangle \approx |\Psi_c^{(0)}(\boldsymbol{r})\rangle + \frac{A_{\mathrm{eff}}(c)}{\varphi_0(0)} G(\varepsilon_c; \boldsymbol{r}, \boldsymbol{0})|0,0\rangle, \tag{88}$$

where the quasi-2D free Green's function $G(\varrho; \boldsymbol{r}, \boldsymbol{r}')$ is given by

$$G(\varrho; \boldsymbol{r}, \boldsymbol{r}') = \frac{1}{\varrho + \mathrm{i}0^+ - \left[H_0^{(2\mathrm{D})} + H_z\right]} \delta(\boldsymbol{r} - \boldsymbol{r}'). \tag{89}$$

Under a procedure similar to that used in Section 3.1, the function $|\Psi_c^{(+)}(\boldsymbol{r})\rangle$ can be approximated as

$$\langle 0,0|\Psi_c^{(+)}(\boldsymbol{r})\rangle \propto \left(\frac{1}{r} - \frac{1}{a_s}\right) \tag{90}$$

in the small-distance region $r_* \lesssim r \ll 1/k$. Thus, we can obtain the result of $A_{\mathrm{eff}}(c)$ and determine the quasi-2D scattering amplitude, which is defined as

$$f^{(\mathrm{Q2D})}(c' \leftarrow c) = -2\pi^2 \int \mathrm{d}\boldsymbol{r}' \langle \Psi_{c'}^{(0)}(\boldsymbol{r}')|\, V_{3\mathrm{D}}(r')\, |\Psi_c^{(+)}(\boldsymbol{r}')\rangle. \tag{91}$$

To understand the behavior of the effective quasi-2D scattering amplitude $f^{(\mathrm{Q2D})}$, we calculate the variation of the mode square of the function

$$F_{\mathrm{eff}} \equiv \frac{f^{(\mathrm{Q2D})}(c' \leftarrow c)}{\langle \psi_{c'}^{(0)}(\boldsymbol{0})|0,0\rangle\langle 0,0|\psi_c^{(0)}(\boldsymbol{0})\rangle}. \tag{92}$$

In Fig. 8, we show the behavior of $|F_{\mathrm{eff}}|^2$ changing with the scattering length when different values of $\epsilon_c - \varepsilon_{\mathrm{th}}(q)$ are taken. Note that, when the value of $\epsilon_c - \varepsilon_{\mathrm{th}}(q)$ is fixed, $|F_{\mathrm{eff}}|^2$ reveals a significant resonance behavior with a_s. Both the resonance point and the maximal amplitude of $|F_{\mathrm{eff}}|^2$ are influenced by the presence of SOC.

Now we consider the two-body bound state in this quasi-2D configuration. In the region $r \gtrsim r_*$, the wave function $|\Psi_b(\boldsymbol{r})\rangle$ can be expressed as

$$|\Psi_b(\boldsymbol{r})\rangle = B' G(E_b; \boldsymbol{r}, \boldsymbol{0})\,|0,0\rangle, \tag{93}$$

where B' is the normalization factor. The state $\Psi_b(\boldsymbol{r})$ with energy E_b of the quasi-2D bound state in the small-distance region also satisfies the Bethe-Peierls boundary

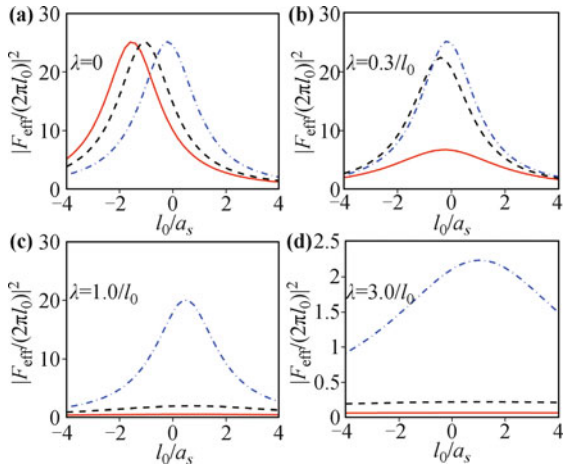

Fig. 8 The behavior of $|F_{\rm eff}|^2$ versus 3D scattering length and $l_0 = 1/\sqrt{\omega_z}$. The results are obtained with zero center-of-mass momentum ($q = 0$), SOC intensities of **(a)** $\lambda = 0$, **(b)** $\lambda = 0.3/l_0$, **(c)** $\lambda = 1/l_0$, and **(d)** $\lambda = 3/l_0$, and quasi-2D scattering energies of $\epsilon_c = -\lambda^2/4 + 0.006\omega_z$ [solid (red) line], $-\lambda^2/4 + 0.02\omega_z$ [dashed (black) line], and $-\lambda^2/4 + 0.2\omega_z$ [dashed-dotted (blue) line]. Reproduced from Ref. [66].

condition

$$\langle 0,0|\,\Psi_b(\boldsymbol{r})\rangle \propto \frac{1}{r} - \frac{1}{a_s}. \tag{94}$$

We can easily prove that this boundary condition is equivalent to the equation

$$-\ln d_{\rm eff}\,(E_b,\boldsymbol{q}) = C + \ln\left(-\frac{i\sqrt{E_b}}{2}\right) + 2\pi\lambda(E_b,\boldsymbol{q}). \tag{95}$$

Here, $C = 0.5772\ldots$ is the Euler gamma number.

In Fig. 9, we show the behavior of binding energy

$$E_{\rm binding} = \varepsilon_{\rm th}(q) - E_b \tag{96}$$

by varying the s-wave scattering length a_s and SOC intensity for $q = 0$. Notice that the value of $E_{\rm binding}$ is increased with SOC intensity λ, indicating that the presence of a Rashba SOC tends to enhance the two-body binding energy. We can qualitatively understand this phenomenon by noting that the density of states in the low-energy limit is increased because the ground state becomes degenerate under SOC.

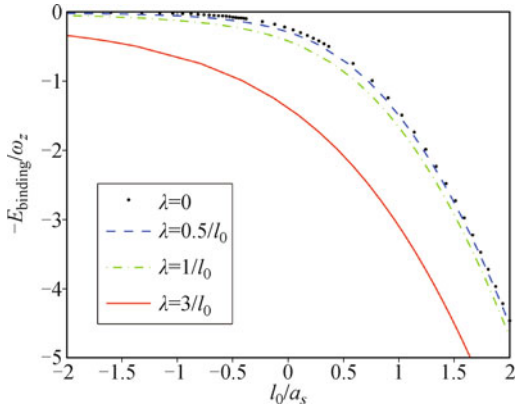

Fig. 9 Binding energy $E_{\rm binding} = \varepsilon_{\rm th}(q) - E_b$ of the quasi-2D two-atom bound state versus the 3D scattering length. In this plot, the center-of-mass momentum $q = 0$ and the SOC intensities are different, as shown in the inset. From Ref. [66].

3.3 Effective Hamiltonian without SOC

In Section 2.1.1, we have introduced a two-channel Hamiltonian to describe a strongly interacting ultracold atomic gas in a transverse trapping potential near a wide Feshbach resonance. Here, we derive an effective low-energy formalism in the form of an effective two-channel model. In the following, for concreteness, we concentrate on a quasi-2D system where the trap frequency ω_z along the z axis is sufficiently strong.

In the dilute-gas limit, one assumes that a quasi-2D atomic density $\rho' \ll 1$ in units of a_t^{-2} and that the situation where three or more atoms are close to each other is rare [26]. Under this condition, the properties of the system are determined by two-body physics and we can neglect three-body collisions. Within the energy regime around the two-body bound-state energy, we know that the occupation of the axially excited state is significant. These modes can be effectively taken into account by introducing the dressed molecular modes in the closed channel, which include the Feshbach molecules as well as atoms in the axially excited states. The short-range interaction between dressed molecules and atoms in the open channel can be modeled by a delta function. The effective low-energy Hamiltonian takes the form

$$\begin{aligned} H_{\rm eff} = &\sum_{\boldsymbol{k}\sigma} \epsilon_{\boldsymbol{k}} a^\dagger_{\boldsymbol{k}\sigma} a_{\boldsymbol{k}\sigma} + \sum_{\boldsymbol{q}} \left(\epsilon_{\boldsymbol{q}}/2 + \delta_b\right) d^\dagger_{\boldsymbol{q}} d_{\boldsymbol{q}} \\ &+ \frac{\alpha_b}{L}\sum_{\boldsymbol{kq}} \left(a^\dagger_{\boldsymbol{k}+\frac{\boldsymbol{q}}{2},\uparrow} a^\dagger_{-\boldsymbol{k}+\frac{\boldsymbol{q}}{2},\uparrow} d_{\boldsymbol{q}} + \text{h.c.}\right) \\ &+ \frac{V_b}{L^2}\sum_{\boldsymbol{kk'q}} a^\dagger_{\boldsymbol{k}+\frac{\boldsymbol{q}}{2},\uparrow} a^\dagger_{-\boldsymbol{k}+\frac{\boldsymbol{q}}{2},\downarrow} a_{-\boldsymbol{k'}+\frac{\boldsymbol{q}}{2},\downarrow} a_{\boldsymbol{k'}+\frac{\boldsymbol{q}}{2},\uparrow}. \end{aligned} \tag{97}$$

Here, $d^\dagger_{\boldsymbol{q}}$ ($d_{\boldsymbol{q}}$) represents the creation (annihilation) operator of the dressed molecule, $a^\dagger_{\boldsymbol{k}\sigma}$ ($a_{\boldsymbol{k}\sigma}$) is the creation (annihilation) operator for the atoms, and $\epsilon_{\boldsymbol{k}} = \hbar^2\boldsymbol{k}^2/2m$. Similar to Eq. (2), we may write a set of renormalization relations for the bare parameters δ_b, α_b, and V_b:

$$\begin{aligned} &V_c^{-1} = \int \frac{\mathrm{d}^2\boldsymbol{k}}{(2\pi)^2}\frac{1}{2\epsilon_{\boldsymbol{k}}+1}, \quad \boldsymbol{\Omega}^{-1} = 1 - V_p V_c^{-1}, \\ &V_p = \boldsymbol{\Omega}^{-1} V_b\,, \quad \alpha_p = \boldsymbol{\Omega}^{-1}\alpha_b\,, \quad \delta_p = \delta_b - \boldsymbol{\Omega}\alpha_p^2 V_c^{-1}. \end{aligned} \tag{98}$$

Importantly, the parameters δ_p, α_p, and V_p should be

chosen such that the effective Hamiltonian $H_{\rm eff}$ should reproduce the same physics as the exact Hamiltonian H at low energies. As we will see in the following, this requirement would allow us to relate the parameters δ_p, α_p, and V_p to the physical parameters in three dimensions.

3.4 Effective Hamiltonian with SOC

Based on Section 3.3, we consider a Rashba-type SOC [69]. The exact Hamiltonian can be written as $H = H_0 + H_I + H_{\rm SOC}$, where H_0 and H_I are the same as those in Section 3.3. The third term, $H_{\rm SOC}$, represents the Rashba-type SOC and takes the form

$$H_{\rm SOC} = -\mathrm{i}\hbar\bar{\lambda}\int d^3\boldsymbol{r}\bar{\psi}^\dagger\left(\sigma_x\partial_x + \sigma_y\partial_y\right)\bar{\psi}. \tag{99}$$

Here, $\bar{\lambda}$ is the SOC intensity, $\sigma_{i=x,y}$ are the Pauli matrices, and $\bar{\psi} = (\psi_\uparrow, \psi_\downarrow)^T$. In momentum space, we have

$$H'_{\rm SOC} = \lambda'\sum_{\boldsymbol{k}}\left[(k_x - \mathrm{i}k_y)a^\dagger_{\boldsymbol{k},\uparrow}a_{\boldsymbol{k},\downarrow} + \text{h.c.}\right], \tag{100}$$

where λ' is the coupling constant of the Rashba SOC.

3.5 Fixing the bare parameters

To relate the parameters δ_p, α_p, V_p, and λ' with the physical parameters in three dimensions, we take into account the following considerations. First, in the low-energy limit, the effective model should reproduce the single-particle dispersion. In other words, we need this Hamiltonian to give the corrent open-channel threshold. Second, when the system is deep in the weak-interaction regime, we should be able to neglect the dressed molecules, as all the atoms should populate the axial ground state. In this situation, the background interaction V_b in the effective model should be related to its three-dimensional counterpart U_b by integrating out the harmonic ground-state degrees of freedom in the axial direction. Finally, when tuning through the Feshbach resonance, we also need the effective Hamiltonian to reproduce the correct two-body physics. As mentioned above, the two-body physics dominates in the dilute-gas limit. The effective theory should produce the same two-body binding energy as the exact one. Furthermore, according to particle conservation, we need the population of dressed molecules to be equal to the population of Feshbach molecules plus that of atoms in the transverse excited states.

To study the two-body problem using the effective theory, we write the general two-body state as

$$|\boldsymbol{\Phi}\rangle_{\boldsymbol{q}} = \left(\beta d^\dagger_{\boldsymbol{q}} + \sum_{\boldsymbol{k}}{}'\sum_{\sigma,\sigma'}\eta^{\sigma\sigma'}_{\boldsymbol{k}}a^\dagger_{\boldsymbol{k}+\boldsymbol{q}/2,\sigma}a^\dagger_{-\boldsymbol{k}+\boldsymbol{q}/2,\sigma'}\right)|0\rangle. \tag{101}$$

Here the summation in $\sum'_{\boldsymbol{k}}$ is taken in the 2D momentum space with $k_y > 0$. Numerically, we find that $q = 0$ for the ground state of a quasi-2D system in the two-body sector. We therefore only discuss the case with $q = 0$ in the following. Solving the Schrödinger equation $H_{\rm eff}|\boldsymbol{\Phi}\rangle_{q=0} = E_b|\boldsymbol{\Phi}\rangle_{q=0}$, we have

$$\left(V_p - \frac{\alpha_p^2}{\delta_p - E_b}\right)^{-1} = \sqrt{2\pi}\sigma_p(E_b), \tag{102}$$

where E_b is the two-body binding energy and the function σ_p is defined as

$$\begin{aligned}\sigma_p(E_b) = &\int\frac{\mathrm{d}^2\boldsymbol{k}}{(2\pi)^{5/2}}\left[\frac{1}{E_b - 2\epsilon_{\boldsymbol{k}} - \dfrac{4(\lambda')^2k^2}{E_b - 2\epsilon_{\boldsymbol{k}}}} + \frac{1}{1+2\epsilon_{\boldsymbol{k}}}\right]\\ &-b\frac{\pi + 2\arctan\dfrac{b+2E_b}{\sqrt{-b(4E_b+b)}}}{8\pi\sqrt{2\pi}\sqrt{-b(4E_b+b)}} + \frac{\ln(-E_b)}{4\pi\sqrt{2\pi}}\end{aligned} \tag{103}$$

with $b \equiv 4(\lambda')^2$.

We may now fix the parameters in the effective model by matching single- and two-body physics as discussed above:

$$\begin{aligned}&\lambda' = \lambda,\\ &V_p^{-1} = \sqrt{2\pi}\left(U_p^{-1} - C_p\right),\\ &\delta_p = E_b - \frac{\sigma_p(E_b)}{\partial\mathcal{P}(E_b)/\partial E_b}\left(1 - \frac{\sigma_p(E_b)}{U_p^{-1} - C_p}\right),\\ &\alpha_p^2 = \frac{1}{\sqrt{2\pi}\partial\mathcal{P}(E_b)/\partial E_b}\left(1 - \frac{\sigma_p(E_b)}{U_p^{-1} - C_p}\right)^2.\end{aligned} \tag{104}$$

Here, the parameters are defined as

$$\begin{aligned}&C_p = S_p(E_b^{\rm inf} + 1/2) - \sigma_p(E_b^{\rm inf}),\\ &\mathcal{P}(E_b) = \left[1/U_p^{\rm eff} - S_p(E_b + 1/2) + \sigma_p(E_b)\right],\\ &U_p^{\rm eff} = U_p - g_p^2/(\nu_p - E_b),\end{aligned} \tag{105}$$

where $E_b^{\rm inf}$ is the two-body binding energy in quasi-two dimensions for $\nu_p \to \infty$. Using Eqs. (98) and (104), we can fix the parameters as functions of the two-body binding energy E_b, which can be tuned via the Feshbach resonance.

Figure 10 shows the parameters δ_p and α_P and the effective interaction $V_p^{\rm eff} \equiv V_p - \alpha_p^2/(\delta_p - E_b)$ for ^{40}K and ^{6}Li as functions of a_s for different SOC intensities λ. The different behaviors for ^{40}K and ^{6}Li are mainly due to the sign difference in their background scattering length.

4 Mean-field study on the effective Hamiltonian

In this section, we demonstrate the utility of the effec-

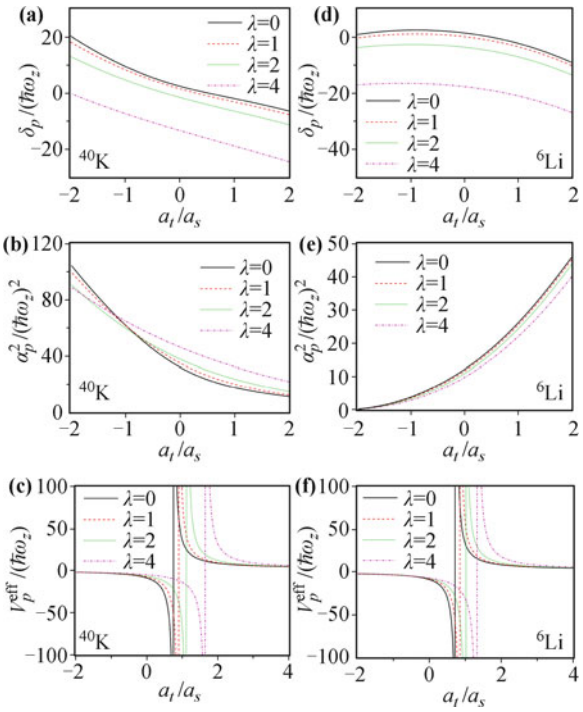

Fig. 10 Parameters in the effective 2D Hamiltonian as functions of a_t/a_a. Reproduced from Ref. [29].

tive two-channel Hamiltonian in dealing with quasi-two-dimensional systems. From these calculations, we show that the population of high-lying states in the tightly confined direction can significantly affect the many-body properties of the system.

4.1 Results in the absence of SOC

In the absence of SOC, the effects of dressed molecules can be seen clearly by comparing results from Eq. (97) (model 2) with those from a simple effective model with a renormalized atom-atom interaction but without dressed molecules (model 1) [70–72].

We first write the effective Hamiltonian for model 1 only in terms of 2D operators $a_{\boldsymbol{k},\sigma}$ and $a^{\dagger}_{\boldsymbol{k},\sigma}$ with pseudo spin σ and transverse momentum $\boldsymbol{k}=(k_x,k_y)$ [40]:

$$H_1=\sum_{\boldsymbol{k},\sigma}\left(\epsilon_{\boldsymbol{k}}-\mu_\rho\right)a^{\dagger}_{\boldsymbol{k},\sigma}a_{\boldsymbol{k},\sigma} +\frac{V_1^{\rm eff}}{L^2}\sum_{\boldsymbol{k},\boldsymbol{k}',\boldsymbol{q}}a^{\dagger}_{\boldsymbol{k},\uparrow}a^{\dagger}_{-\boldsymbol{k}+\boldsymbol{q},\downarrow}a_{\boldsymbol{k}',\downarrow}a_{-\boldsymbol{k}'+\boldsymbol{q},\uparrow}, \tag{106}$$

where $\epsilon_{\boldsymbol{k}}=\hbar^2k^2/(2m)$ is the 2D dispersion relation for fermions with mass m, μ_ρ is the chemical potential, and L^2 is the quantization area. The bare parameter $V_1^{\rm eff}$ is subject to the 2D renormalization relation $\left[V_1^{\rm eff}\right]^{-1}=\left[V_{1p}^{\rm eff}\right]^{-1}-L^{-2}\sum_{\boldsymbol{k}}\left(2\epsilon_{\boldsymbol{k}}+\hbar\omega_z\right)^{-1}$. Here $V_{1p}^{\rm eff}=V_{1p}^{\rm eff}(a_s,a_z)$ is a function of the 3D scattering length a_s and the characteristic length scale for axial motion $a_z\equiv\sqrt{\hbar/(m\omega_z)}$ [40]. Under the local density approximation (LDA), the chemical potential μ_ρ depends on the radial coordinate $\boldsymbol{r}=(x,y)$. Here, we choose $\hbar\omega_z$ as the energy unit.

The zero-temperature thermodynamic potential is

$$\Omega=-\frac{\Delta^2}{V_1^{\rm eff}}+\frac{1}{L^2}\sum_{\boldsymbol{k}}\left(\epsilon_{\boldsymbol{k}}-\mu_\rho-E_{\boldsymbol{k}}\right), \tag{107}$$

where $\Delta\equiv(V_1^{\rm eff}/L^2)\sum_{\boldsymbol{k}}\langle a_{\boldsymbol{k},\downarrow}a_{-\boldsymbol{k},\uparrow}\rangle$ is the BCS order parameter and $E_{\boldsymbol{k}}=\sqrt{(\epsilon_{\boldsymbol{k}}-\mu_\rho)^2+\Delta^2}$ is the quasiparticle excitation spectrum. Then, from the relation $\partial\Omega/\partial\Delta=0$ and $n=-\partial\Omega/\partial\mu$, we can obtain the gap and number equations

$$\frac{1}{V_{1p}^{\rm eff}(a_s,a_z)}=\frac{\ln\left(-\mu_\rho+\sqrt{\mu_\rho^2+\Delta^2}\right)}{4\pi a_z^2}, \tag{108}$$

$$n=\frac{\mu_\rho+\sqrt{\mu_\rho^2+\Delta^2}}{2\pi a_z^2}. \tag{109}$$

We may then write the chemical potential $\mu_\rho(\boldsymbol{r})=\mu_0-V(\boldsymbol{r})$, where the harmonic trapping potential is $V(\boldsymbol{r})=(\omega_\perp/\omega_z)^2r^2/(2a_z^2)$ and μ_0 is the chemical potential at the center of the trap. We can easily show that the spatial density profile is a parabola, $n(\boldsymbol{r})=(\omega_\perp/\omega_z)^2(R_{\rm TF}^2-r^2)/(2\pi a_z^4)$, where $R_{\rm TF}=\sqrt{2\mu_0}a_z(\omega_z/\omega_\perp)$ is the Thomas-Fermi cloud size. Taking into account total particle number conservation, we have a constant cloud size $R_{\rm TF}=R_{\rm BCS}\equiv\sqrt{2\omega_z/\omega_\perp}(N)^{1/4}a_z$, where $N=\int n(\boldsymbol{r})\mathrm{d}^2\boldsymbol{r}$ is the total number of particles in the trap. We find that the size $R_{\rm BCS}$ is independent of the 3D scattering length a_s. This result is obviously inconsistent with the physical picture of the BCS-BEC crossover in a quasi-2D system. On the BEC side of the Feshbach resonance, fermions will form tightly bound pairs, and the pair size $a_{\rm pair}\ll a_z$ and binding energy $|E_b|\gg\hbar\omega_z$. In this situation, the cloud size is expected to be small.

Then we adopt model 2 to characterize the system. The Hamiltonian of model 2 is shown in Eq. (97). We introduce a new order parameter $\Delta\equiv\alpha_b\langle d_0\rangle/L+(V_b/L^2)\sum_{\boldsymbol{k}}\langle a_{\boldsymbol{k},\downarrow}a_{-\boldsymbol{k},\uparrow}\rangle$. Using the same means, we can obtain the mean-field gap and number equations

$$\frac{1}{V_{2p}^{\rm eff}(2\mu_\rho)}=\frac{\ln\left(-\mu_\rho+\sqrt{\mu_\rho^2+\Delta^2}\right)}{4\pi a_z^2}, \tag{110}$$

$$n=\frac{\mu_\rho+\sqrt{\mu_\rho^2+\Delta^2}}{2\pi a_z^2}+2\Delta^2\frac{\partial[V_{2,\rm p}^{\rm eff}(x)]^{-1}}{\partial x}\bigg|_{x=2\mu_\rho}, \tag{111}$$

where the inverse of the effective interaction can be re-

lated to the 3D physical parameters through the relation [27]

$$\left[V_{2p}^{\rm eff}(x)\right]^{-1} = \left[V_b + \frac{\alpha_b^2}{x-\delta_b}\right]^{-1} + \frac{1}{L^2}\sum_{\boldsymbol{k}} \frac{1}{2\epsilon_{\boldsymbol{k}} + \hbar\omega_z}$$
$$= \frac{\sqrt{2\pi}}{a_z^2}\left[\left(U_p + \frac{g_p^2}{x-\gamma_p}\right)^{-1} - S_p(x) + \sigma_p'(x)\right]. \quad (112)$$

The functions in Eq. (112) take the form

$$S_p(x) = \frac{-1}{4\sqrt{2}\pi}\int_0^\infty {\rm d}s \left[\frac{\Gamma(s-x/2)}{\Gamma(s+1/2-x/2)} - \frac{1}{\sqrt{s}}\right],$$
$$\sigma_p'(x) = \frac{\ln|x|}{4\pi\sqrt{2\pi}}, \quad (113)$$

where $\Gamma(x)$ is the gamma function.

We then solve the mean-field gap and number equations under model 1 and model 2, respectively. In our calculation, we use the parameters that have been introduced in Section 2.1.1 for ^{40}K and ^{6}Li. Figure 11 shows a series of results for both ^{40}K and ^{6}Li. A smooth crossover from the BCS (right) to the BEC (left) regimes is shown. We find that the results for ^{40}K (dashed) and ^{6}Li (solid) are very similar near the resonance. The results of model 1 and model 2 are significantly different in this figure, especially on the BEC side. From these results, we can conclude that we cannot directly apply model 1 to describe the BCS-BEC crossover in a quasi-2D system where the dressed molecules have been neglected.

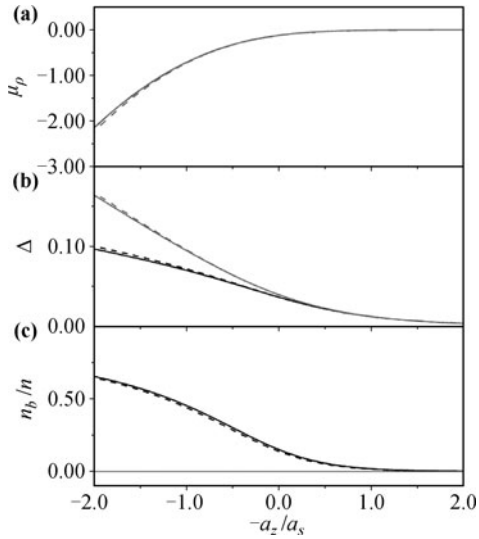

Fig. 11 BCS-BEC crossover behavior of a uniform quasi-2D Fermi gas at zero temperature, showing **(a)** the chemical potential μ, **(b)** the gap Δ, both in units of $\hbar\omega_z$, and **(c)** the dressed-molecule fraction n_b/n. Significant differences between model 1 (*gray*) and model 2 (*black*) are present for both ^{40}K (*dashed*) and ^{6}Li (*solid*). Parameters used in these plots are $\omega_z = 2\pi \times 62$ kHz and $na_z^2 = 0.001$. Reproduced from Ref. [55].

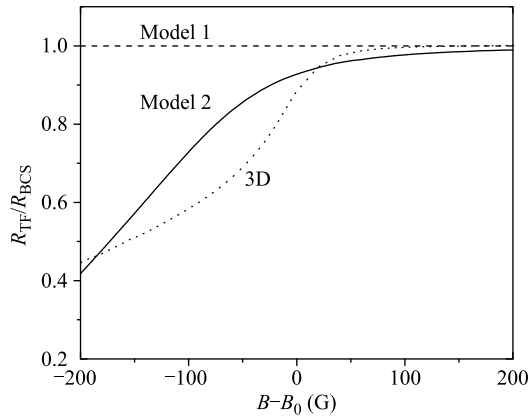

Fig. 12 Thomas-Fermi cloud size of ^{6}Li in the quasi-2D system within the BCS-BEC crossover. The results of $R_{\rm TF}$ are normalized to $R_{\rm BCS}$, which is the cloud size of the noninteracting Fermi gas. The results of both model 1 (*dashed*) and model 2 (*solid*) are shown. Reproduced from Ref. [55].

Figure 12 shows the Thomas-Fermi cloud size under the total particle conservation condition. We can clearly see that for model 2 (solid curve) the cloud size is no longer a constant, whereas model 1 predicts a constant one (dashed curve). In model 2, when the Feshbach resonance is crossed, the cloud size decreases from the value $R_{\rm BCS}$, which is the size of a noninteracting Fermi gas in the BCS limit, to the 3D results (dotted curve) in the BEC limit. This result successfully recovers the physics on both the BCS and BEC sides of the Feshbach resonance.

4.2 Dressed molecules under SOC

Under SOC, the impacts of the dressed molecules can be more significant. Here, we consider a quasi-2D Fermi gas with Rashba SOC and an effective Zeeman field, where a topological superfluid (TSF) can be stabilized. Assuming a slow-varying harmonic potential in the x-y plane, we apply the LDA $\mu_\rho(\tilde{\boldsymbol{r}}) = \mu_\rho(0) - V(\tilde{\boldsymbol{r}})$, where $\tilde{r} = \sum_i r_i^2/R_i^2$, $R_i = a_t\omega_z/\omega_i$ is the unit of length along the ith $(i = x, y)$ direction, and $V(\tilde{\boldsymbol{r}}) = \tilde{r}^2/2$.

The zero-temperature thermodynamic potential can be written at the mean-field level [73] as

$$\Omega = -\frac{|\Delta|^2}{V_p^{\rm eff}} + \frac{1}{2}\sum_{\boldsymbol{k},s=\pm}\left(\xi_s - E_{\boldsymbol{k},s}\right), \quad (114)$$

where the order parameter of the two-channel model has been defined in Section 4.1 and $V_p^{\rm eff} \equiv V_p - \alpha_p^2/(\delta_p - E_b)$. The dispersion relations for quasiparticles with SOC are given by [73]

$$E_{\boldsymbol{k},\pm} = \sqrt{\xi_{\boldsymbol{k}}^2 + \lambda^2k^2 + |\Delta|^2 + h^2 \pm 2E_0}, \quad (115)$$

where $E_0 = \sqrt{h^2\left(\xi_{\boldsymbol{k}}^2 + |\Delta|^2\right) + \lambda^2\xi_{\boldsymbol{k}}^2 k^2}$ and $\xi_{\boldsymbol{k}} = \epsilon_{\boldsymbol{k}} - \mu_\rho(\tilde{\boldsymbol{r}})$.

We can obtain the local chemical potentials form the dimensionless number equations

$$\tilde{N} = \int \mathrm{d}^2\tilde{\boldsymbol{r}}[\tilde{n}_\uparrow(\tilde{\boldsymbol{r}}) + \tilde{n}_\downarrow(\tilde{\boldsymbol{r}})], \tag{116}$$

$$P = \frac{1}{\tilde{N}}\int \mathrm{d}^2\tilde{\boldsymbol{r}}[\tilde{n}_\uparrow(\tilde{\boldsymbol{r}}) - \tilde{n}_\downarrow(\tilde{\boldsymbol{r}})], \tag{117}$$

where $\tilde{n}_\uparrow = -(\partial\Omega/\partial\mu_\rho + \partial\Omega/\partial h)/2$, $\tilde{n}_\downarrow = -(\partial\Omega/\partial\mu_\rho - \partial\Omega/\partial h)/2$, and $\tilde{N} = N\omega_x\omega_y/\omega_z^2$, with N the total particle number in the trap. By solving these equations while minimizing the local thermodynamic potential, we can obtain the density distribution. The population of the dressed molecules has the form [74]

$$\tilde{n}_b(\tilde{\boldsymbol{r}}) = \langle d_0^\dagger d_0\rangle = |\Delta(\tilde{\boldsymbol{r}})|^2\left[\alpha_p - \frac{U_p(\delta_p - 2\mu_\rho(\tilde{\boldsymbol{r}}))}{\alpha_p}\right]^{-2}. \tag{118}$$

Importantly, when the Zeeman field h crosses $\sqrt{\mu_\rho^2 + \Delta^2}$ from below, the system can undergo a phase transition from the superfluid (SF) state to the TSF state [73]. Hence, we can define the TSF phase in the trap where $h > \sqrt{\mu_\rho^2(\tilde{\boldsymbol{r}}) + |\Delta(\tilde{\boldsymbol{r}})|^2}$. The order parameter of the TSF state is the same as the one of the SF state, because these two states have the same symmetry and cannot be separated by spontaneous symmetry breaking.

In Fig. 13, we plot the density distributions with different SOC intensities λ, 3D scattering lengths a_s and polarizations P. Both the results from the two-channel model and those from the single-channel model are shown. We find that the density distribution can be significantly changed by the dressed molecules. In the presence of dressed molecules, there is a difference in the in-trap phase structure where the phase boundaries between the SF phase at the center and the TSF phase at the edge are shifted.

Although the difference in density distributions of the two models is more significant on the BEC side, the dressed molecules also have significant effects near the resonance point or even on the BCS side, in contrast to the case without SOC [55]. We can understand this phenomenon by combining the effects of SOC and population imbalance. In a polarized Fermi gas, the population imbalance is usually accounted for by the normal phase toward the trap edge or by exotic superfluid phases that support polarization, e.g., the Fulde-Ferrell-Larkin-Ovchinnikov (FFLO) phase [75, 76], the breached pair (BP) phase [77], or the TSF phase with SOC [25, 78]. As discussed above in the two-body physics, SOC will increase the two-body binding energy and, hence, more

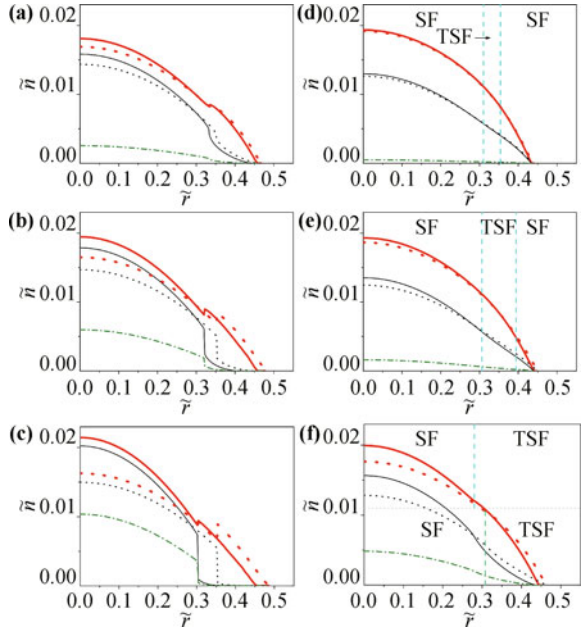

Fig. 13 Density distribution for different interaction strengths with fixed SOC and polarization: **(a)**–**(c)** $\lambda \sim 0.14$, $P \sim 0.20$; **(d)**–**(f)** $\lambda \sim 0.22$, $P \sim 0.27$. In all cases, $\omega_x/\omega_z = 10^{-3}$ and $N \sim 10^4$, with (a) $a_t/a_s \sim -0.36$, (b) $a_t/a_s \sim 0.04$, (c) $a_t/a_s \sim 0.34$, (d) $a_t/a_s \sim -1$, (e) $a_t/a_s \sim -0.5$, and (f) $a_t/a_s \sim 0$; The bold red (thin black) dotted curves are the density distribution of spin–up (spin–down) atoms in the single-channel model, and the solid curves are the density distribution in the effective two-channel model. The distributions for atoms in the closed channel are shown with the dash-dotted (green) lines. Reproduced from Ref. [29].

atoms will populate the axial harmonic excited states. In other words, SOC will enhance the effects of dressed molecules. However, the dressed molecules do not support polarization. Therefore, the density distribution of the system with dressed molecules has to be modified to accommodate the total polarization.

5 Conclusions

As we have demonstrated in this review, few-body physics in quasi-low-dimensional atomic gases can be quite different from the physics in a purely low dimensional system. The extra degrees of freedom in the tightly confined dimensions may significantly affect various properties of the system once they are occupied. The occupation of these states occur, when, for example, the two-body binding energy becomes comparable to the trapping frequency of the tight confinement. Therefore, one must be careful in treating quasi-low-dimensional atomic gases, particularly when they are close to the Feshbach resonance or on the BEC side.

These considerations become even more relevant when the atoms are subject to a synthetic SOC. By modifying

the single-particle dispersion spectra, SOC affects both the two-body bound states and the scattering states. In a quasi-1D atomic gas, parameters of a NIST-type SOC can shift the positions of the CIR and have significant impact on the two-body bound-state energy, whereas in a quasi-2D atomic gas, a Rashba-type SOC increases the two-body bound-state energy, enhances the occupation of the excited states in the tightly confined dimension, and thus drives the system further away from a purely low dimensional atomic gas. By adopting an effective low-energy two-channel Hamiltonian, one may capture the effects of the excited-state occupation in the tightly confined dimensions by modeling them with dressed molecules in the closed channel. With the bare parameters of the two-channel model fixed by two-body calculations, one may then apply the effective low-energy theory to characterize many-body properties. While we see that the inclusion of the extra degrees of freedom in a quasi-2D Fermi gas under Rashba SOC and an effective out-of-plane Zeeman field can lead to an enhanced stability of the topological superfluid state, application of the two-channel model may reveal more interesting many-body properties of quasi-low-dimensional atomic gases.

Acknowledgements This work was supported by the National Key Basic Research Program of China (Grant No. 2013CB922000), the National Programs for Fundamental Research and Development (Grant Nos. 2011CB921200 and 2011CBA00200), and the National Natural Science Foundation of China (Grant Nos. 11274009, 11434001, 60921091, 11404106, and 11374283). W. Y. acknowledges support from the "Strategic Priority Research Program (B)" of the Chinese Academy of Sciences, Grant No. XDB01030200. W. Z. thanks the Research Funds of Renmin University of China (Grant No. 10XNL016) and the Simons Foundation for support.

References

1. Y. J. Lin, R. L. Compton, A. R. Perry, W. D. Phillips, J. V. Porto, and I. B. Spielman, Bose–Einstein condensate in a uniform light-induced vector potential, *Phys. Rev. Lett.* 102(13), 130401 (2009)
2. Y. J. Lin, K. Jiménez-García, and I. B. Spielman, Spin–orbit-coupled Bose–Einstein condensates, *Nature* 471(7336), 83 (2011)
3. J. Y. Zhang, S. C. Ji, Z. Chen, L. Zhang, Z. D. Du, B. Yan, G. S. Pan, B. Zhao, Y. J. Deng, H. Zhai, S. Chen, and J. W. Pan, Collective dipole oscillations of a spin–orbit coupled Bose–Einstein condensate, *Phys. Rev. Lett.* 109(11), 115301 (2012)
4. C. Qu, C. Hamner, M. Gong, C. Zhang, and P. Engels, Non-equilibrium spin dynamics and Zitterbewegung in quenched spin–orbit coupled Bose–Einstein condensates, *Phys. Rev. A* 88, 021604(R) (2013)
5. S. C. Ji, J. Y. Zhang, L. Zhang, Z. D. Du, W. Zheng, Y. J. Deng, H. Zhai, S. Chen, and J. W. Pan, Experimental determination of the finite-temperature phase diagram of a spin–orbit coupled Bose gas, *Nat. Phys.* 10(4), 314 (2014)
6. P. Wang, Z. Q. Yu, Z. Fu, J. Miao, L. Huang, S. Chai, H. Zhai, and J. Zhang, Spin-orbit coupled degenerate Fermi gases, *Phys. Rev. Lett.* 109(9), 095301 (2012)
7. L. W. Cheuk, A. T. Sommer, Z. Hadzibabic, T. Yefsah, W. S. Bakr, and M. W. Zwierlein, Spin-injection spectroscopy of a spin–orbit coupled Fermi gas, *Phys. Rev. Lett.* 109(9), 095302 (2012)
8. Z. Fu, L. Huang, Z. Meng, P. Wang, L. Zhang, S. Zhang, H. Zhai, P. Zhang, and J. Zhang, Production of Feshbach molecules induced by spin–orbit coupling in Fermi gases, *Nat. Phys.* 10(2), 110 (2014)
9. P. J. Wang and J. Zhang, Spin–orbit coupling in Bose–Einstein condensate and degenerate Fermi gases, *Front. Phys.* 9(5), 612 (2014)
10. H. Zhai, Spin–orbit coupled quantum gases, *Int. J. Mod. Phys. B* 26(01), 1230001 (2012)
11. V. Galitski and I. B. Spielman, Spin–orbit coupling in quantum gases, *Nature* 494(7435), 49 (2013)
12. X. Zhou, Y. Li, Z. Cai, and C. Wu, Unconventional states of bosons with the synthetic spin–orbit coupling, *J. Phys. B* 46(13), 134001 (2013)
13. N. Goldman, G. Juzeliūnas, P. Öhberg, and I. B. Spielman, Light-induced gauge fields for ultracold atoms, *Rep. Prog. Phys.* 77(12), 126401 (2014)
14. H. Zhai, Degenerate quantum gases with spin–orbit coupling: A review, *Rep. Prog. Phys.* 78(2), 026001 (2015)
15. J. Zhang, H. Hu, X. J. Liu, and H. Pu, Fermi gases with synthetic spin–orbit coupling, *Annu. Rev. Cold At. Mol.* 2, 81 (2014)
16. Y. Xu and C. Zhang, Topological Fulde–Ferrell superfluids of a spin–orbit coupled Fermi gas, *Int. J. Mod. Phys. B* 29(01), 1530001 (2015)
17. W. Yi, W. Zhang, and X. Cui, Pairing superfluidity in spin–orbit coupled ultracold Fermi gases, *Sci. China - Phys. Mech. Astron.* 58(1), 014201 (2015)
18. J. P. Vyasanakere and V. B. Shenoy, Bound states of two spin-1/2 fermions in a synthetic non-Abelian gauge field, *Phys. Rev. B* 83(9), 094515 (2011)
19. J. P. Vyasanakere, S. Zhang, and V. B. Shenoy, BCS–BEC crossover induced by a synthetic non-Abelian gauge field, *Phys. Rev. B* 84(1), 014512 (2011)

20. X. Cui, Mixed-partial-wave scattering with spin–orbit coupling and validity of pseudopotentials, *Phys. Rev. A* 85(2), 022705 (2012)
21. Z. F. Xu and L. You, Dynamical generation of arbitrary spin–orbit couplings for neutral atoms, *Phys. Rev. A* 85(4), 043605 (2012)
22. F. Wu, R. Zhang, T. S. Deng, W. Zhang, W. Yi, and G. C. Guo, BCS–BEC crossover and quantum phase transition in an ultracold Fermi gas under spin–orbit coupling, *Phys. Rev. A* 89(6), 063610 (2014)
23. Z. Y. Shi, X. Cui, and H. Zhai, Universal trimers induced by spin–orbit coupling in ultracold Fermi gases, *Phys. Rev. Lett.* 112(1), 013201 (2014)
24. X. Cui, and W. Yi, Universal Borromean binding in spin–orbit-coupled ultracold fermi gases, *Phys. Rev. X* 4(3), 031026 (2014)
25. M. Sato, Y. Takahashi, and S. Fujimoto, Non-Abelian topological order in s-wave superfluids of ultracold fermionic atoms, *Phys. Rev. Lett.* 103(2), 020401 (2009)
26. J. P. Kestner and L. M. Duan, Conditions of low dimensionality for strongly interacting atoms under a transverse trap, *Phys. Rev. A* 74(5), 053606 (2006)
27. J. P. Kestner and L. M. Duan, Effective low-dimensional Hamiltonian for strongly interacting atoms in a transverse trap, *Phys. Rev. A* 76(6), 063610 (2007)
28. Z. Q. Yu and H. Zhai, Spin–orbit coupled Fermi gases across a Feshbach resonance, *Phys. Rev. Lett.* 107(19), 195305 (2011)
29. R. Zhang, F. Wu, J. R. Tang, G. C. Guo, W. Yi, and W. Zhang, Significance of dressed molecules in a quasi-two-dimensional Fermi gas with spin–orbit coupling, *Phys. Rev. A* 87(3), 033629 (2013)
30. T. Stöferle, H. Moritz, K. Günter, M. Köhl, and T. Esslinger, Molecules of fermionic atoms in an optical lattice, *Phys. Rev. Lett.* 96(3), 030401 (2006)
31. B. Paredes, A. Widera, V. Murg, O. Mandel, S. Fölling, I. Cirac, G. V. Shlyapnikov, T. W. Hänsch, and I. Bloch, Tonks–Girardeau gas of ultracold atoms in an optical lattice, *Nature* 429(6989), 227 (2004)
32. T. Kinoshita, T. Wenger, and D. S. Weiss, Observation of a one-dimensional Tonks–Girardeau gas, *Science* 305(5687), 1125 (2004)
33. M. Köhl, H. Moritz, T. Stöferle, K. Günter, and T. Esslinger, Fermionic atoms in a three dimensional optical lattice: Observing Fermi surfaces, dynamics, and interactions, *Phys. Rev. Lett.* 94(8), 080403 (2005)
34. Y. Castin, Simple theoretical tools for low dimension Bose gases, *J. Phys. IV* 116, 89 (2004)
35. D. E. Sheehy and L. Radzihovsky, Quantum decoupling transition in a one-dimensional Feshbach-resonant superfluid, *Phys. Rev. Lett.* 95(13), 130401 (2005)
36. E. Orignac and R. Citro, Phase transitions in the boson–fermion resonance model in one dimension, *Phys. Rev. A* 73(6), 063611 (2006)
37. M. Olshanii, Atomic scattering in the presence of an external confinement and a gas of impenetrable bosons, *Phys. Rev. Lett.* 81(5), 938 (1998)
38. T. Bergeman, M. G. Moore, and M. Olshanii, Atom–atom scattering under cylindrical harmonic confinement: Numerical and analytic studies of the confinement induced resonance, *Phys. Rev. Lett.* 91(16), 163201 (2003)
39. T. Busch, B. G. Englert, K. Rzażwski, and M. Wilkens, Two cold atoms in a harmonic trap, *Found. Phys.* 28(4), 549 (1998)
40. D. S. Petrov, M. Holzmann, and G. V. Shlyapnikov, Bose–Einstein condensation in quasi-2D trapped gases, *Phys. Rev. Lett.* 84(12), 2551 (2000)
41. D. S. Petrov and G. V. Shlyapnikov, Interatomic collisions in a tightly confined Bose gas, *Phys. Rev. A* 64(1), 012706 (2001)
42. P. O. Fedichev, M. J. Bijlsma, and P. Zoller, Extended molecules and geometric scattering resonances in optical lattices, *Phys. Rev. Lett.* 92(8), 080401 (2004)
43. M. Holland, S. J. J. M. F. Kokkelmans, M. L. Chiofalo, and R. Walser, Resonance superfluidity in a quantum degenerate Fermi gas, *Phys. Rev. Lett.* 87(12), 120406 (2001)
44. M. H. Szymańska, K. Góral, T. Köhler, and K. Burnett, Conventional character of the BCS–BEC crossover in ultracold gases of K^{40}, *Phys. Rev. A* 72(1), 013610 (2005)
45. Q. Chen, J. Stajic, S. Tan, and K. Levin, BCS–BEC crossover: From high temperature superconductors to ultracold superfluids, *Phys. Rep.* 412(1), 1 (2005)
46. Q. Chen and J. Wang, Pseudogap phenomena in ultracold atomic Fermi gases, *Front. Phys.* 9(5), 570 (2014)
47. L. M. Duan, Effective Hamiltonian for fermions in an optical lattice across a Feshbach resonance, *Phys. Rev. Lett.* 95(24), 243202 (2005)
48. R. B. Diener and T. L. Ho, Fermions in optical lattices swept across Feshbach resonances, *Phys. Rev. Lett.* 96(1), 010402 (2006)
49. C. A. Regal, M. Greiner, and D. S. Jin, Observation of resonance condensation of fermionic atom pairs, *Phys. Rev. Lett.* 92(4), 040403 (2004)
50. K. Huang, Statistical Mechanics, 2nd Ed., New York: Wiley, 1987
51. L. Tonks, The complete equation of state of one, two and three-dimensional gases of hard elastic spheres, *Phys. Rev.* 50(10), 955 (1936)
52. H. Moritz, T. Stöferle, K. Günter, M. Köhl, and T. Esslinger, Confinement induced molecules in a 1D Fermi gas, *Phys. Rev. Lett.* 94(21), 210401 (2005)
53. J. K. Chin, D. E. Miller, Y. Liu, C. Stan, W. Setiawan, C. Sanner, K. Xu, and W. Ketterle, Evidence for superfluidity of ultracold fermions in an optical lattice, *Nature* 443(7114), 961 (2006)
54. Z. Hadzibabic, P. Krüger, M. Cheneau, B. Battelier, and J. Dalibard, Berezinskii–Kosterlitz–Thouless crossover in a trapped atomic gas, *Nature* 441(7097), 1118 (2006)

55. W. Zhang, G. D. Lin, and L. M. Duan, BCS–BEC crossover of a quasi-two-dimensional Fermi gas: The significance of dressed molecules, *Phys. Rev. A* 77(6), 063613 (2008)
56. P. Dyke, E. D. Kuhnle, S. Whitlock, H. Hu, M. Mark, S. Hoinka, M. Lingham, P. Hannaford, and C. J. Vale, Crossover from 2D to 3D in a weakly interacting Fermi gas, *Phys. Rev. Lett.* 106(10), 105304 (2011)
57. A. A. Abrikosov, L. P. Gorkov, and I. E. Dzyaloshinski, Methods of Quantum Field Theory in Statistical Physics, 2nd Ed., New York: Dover, 1975
58. L. D. Landau and E. M. Lifshitz, Quantum Mechanics, 3rd Ed., Oxford: Butterworth–Heinemann, 1999
59. Y. Kagan, B. V. Svistunov, and G. V. Shlyapnikov, Influence on inelastic processes of the phase transition in a weakly collisional two-dimensional Bose gas, *Sov. Phys. JETP* 66, 480 (1987)
60. R. P. Feynman and A. R. Hibbs, Quantum Mechanics and Path Integrals, 2ndEd., New York: McGraw-Hill, 1995
61. W. Zhang and P. Zhang, Confinement-induced resonances in quasi-one-dimensional traps with transverse anisotropy, *Phys. Rev. A* 83(5), 053615 (2011)
62. A. P. Prudnikov, Y. A. Brychkov, and O. I. Marichev, Integrals and Series, 2nd Ed., New York: Gordon and Breach, 1986
63. Z. Idziaszek and T. Calarco, Analytical solutions for the dynamics of two trapped interacting ultracold atoms, *Phys. Rev. A* 74(2), 022712 (2006)
64. X. J. Liu and H. Hu, Topological superfluid in one-dimensional spin–orbit-coupled atomic Fermi gases, *Phys. Rev. A* 85(3), 033622 (2012)
65. J. R. Taylor, Scattering Theory, 2nd Ed., New York: Wiley, 1972
66. P. Zhang, L. Zhang, and W. Zhang, Interatomic collisions in two-dimensional and quasi-two-dimensional confinements with spin–orbit coupling, *Phys. Rev. A* 86(4), 042707 (2012)
67. Y. C. Zhang, S. W. Song, and W. M. Liu, The confinement induced resonance in spin–orbit coupled cold atoms with Raman coupling, *Sci. Rep.* 4, 4992 (2014)
68. R. Zhang and W. Zhang, Effective Hamiltonians for quasi-one-dimensional Fermi gases with spin–orbit coupling, *Phys. Rev. A* 88(5), 053605 (2013)
69. L. Dell'Anna, G. Mazzarella, and L. Salasnich, Condensate fraction of a resonant Fermi gas with spin–orbit coupling in three and two dimensions, *Phys. Rev. A* 84(3), 033633 (2011)
70. A. J. Leggett, Modern Trends in the Theory of Condensed Matter, 2nd Ed., Berlin: Springer-Verlag, 1980
71. P. Nozières and S. Schmitt-Rink, Bose condensation in an attractive fermion gas: From weak to strong coupling superconductivity, *J. Low Temp. Phys.* 59(3), 195 (1985)
72. C. A. R. S. de Melo, M. Randeria, and J. R. Engelbrecht, Crossover from BCS to Bose superconductivity– transition temparetaure and time-dependent Ginzburg–Landau theory, *Phys. Rev. Lett.* 71, 3202 (1993)
73. J. Zhou, W. Zhang, and W. Yi, Topological superfluid in a trapped two-dimensional polarized Fermi gas with spin–orbit coupling, *Phys. Rev. A* 84(6), 063603 (2011)
74. W. Yi and L. M. Duan, BCS–BEC crossover and quantum phase transition for Li^6 and K^{40} atoms across the Feshbach resonance, *Phys. Rev. A* 73(6), 063607 (2006)
75. P. Fulde and R. A. Ferrell, Superconductivity in a strong spin-exchange field, *Phys. Rev.* 135(3A), A550 (1964)
76. A. I. Larkin and Y. N. Ovchinnikov, Inhomogeneous state of superconductors, *Sov. Phys. JETP* 20, 762 (1965)
77. W. V. Liu and F. Wilczek, Interior gap superfluidity, *Phys. Rev. Lett.* 90(4), 047002 (2003)
78. C. Zhang, S. Tewari, R. M. Lutchyn, and S. Das Sarma, p_x+ip_y superfluid from s-wave interactions of fermionic cold atoms, *Phys. Rev. Lett.* 101(16), 160401 (2008)